AD-A067 185 RESEARCH TRIANGLE INST RESEARCH TRIANGLE PARK N C F/G 11/9
DETERMINATION OF CROSSLINKING IN HIGH TG POLYMERS.(U)
JAN 79 A SCHINDLER, N MOROSOFF F33615-77-C-5195
UNCLASSIFIED AFML-TR-78-186 NL

END
DATE FILMED
6-79
DDC

LEVEL II

AFML-TR-78-186

(12)

DETERMINATION OF CROSSLINKING IN HIGH T_g POLYMERS

RESEARCH TRIANGLE INSTITUTE
P. O. BOX 12194
RESEARCH TRIANGLE PART, N. C. 27709

JANUARY 1979

TECHNICAL REPORT AFML-TR-78-186
Interim Report for 15 October 1977 – 15 October 1978

Approved for public release; distribution unlimited.

AIR FORCE AVIONICS LABORATORY
AIR FORCE WRIGHT AERONAUTICAL LABORATORIES
AIR FORCE SYSTEMS COMMAND
WRIGHT-PATTERSON AIR FORCE BASE, OHIO 45433

NOTICE

When Government drawings, specifications, or other data are used for any purpose other than in connection with a definitely related Government procurement operation, the United States Government thereby incurs no responsibility nor any obligation whatsoever; and the fact that the government may have formulated, furnished, or in any way supplied the said drawings, specifications, or other data, is not to be regarded by implication or otherwise as in any manner licensing the holder or any other person or corporation, or conveying any rights or permission to manufacture, use, or sell any patented invention that may in any way be related thereto.

This report has been reviewed by the Information Office (OI) and is releasable to the National Technical Information Service (NTIS). At NTIS, it will be available to the general public, including foreign nations.

This technical report has been reviewed and is approved for publication.

FREEMAN F. BENTLEY
Project Monitor

R. L. VAN DEUSEN, Chief
Polymer Branch
Nonmetallic Materials Division

FOR THE COMMANDER

J. M. KELBLE, Chief
Nonmetallic Materials Division

"If your address has changed, if you wish to be removed from our mailing list, or if the addressee is no longer employed by your organization please notify AFML/MBP ,*W-PAFB, OH 45433 to help us maintain a current mailing list".*

Copies of this report should not be returned unless return is required by security considerations, contractual obligations, or notice on a specific document.

AIR FORCE/56780/27 March 1979 — 100

SECURITY CLASSIFICATION OF THIS PAGE (When Data Entered)

REPORT DOCUMENTATION PAGE

READ INSTRUCTIONS BEFORE COMPLETING FORM

(18) 1. REPORT NUMBER: AFML-TR-78-168 (19) TR-78-486

2. GOVT ACCESSION NO.

3. RECIPIENT'S CATALOG NUMBER

(6) 4. TITLE (and Subtitle): DETERMINATION OF CROSSLINKING IN HIGH T_g POLYMERS

5. TYPE OF REPORT & PERIOD COVERED: Interim Report for the Period 10/15/77 - 10/15/78

6. PERFORMING ORG. REPORT NUMBER

(10) 7. AUTHOR(s): ~~Dr.~~ A. Schindler, ~~Dr.~~ N. Morosoff

(15) 8. CONTRACT OR GRANT NUMBER(s): F33615-77-C-5195

9. PERFORMING ORGANIZATION NAME AND ADDRESS:
Research Triangle Institute
P. O. Box 12194
Research Triangle Park, N. C. 27709

10. PROGRAM ELEMENT, PROJECT, TASK AREA & WORK UNIT NUMBERS

11. CONTROLLING OFFICE NAME AND ADDRESS:
Air Force Materials Laboratory (MBP)
Air Force Systems Command
Wright-Patterson Air Force Base, OH 45433

12. REPORT DATE: November, 1978

13. NUMBER OF PAGES: 77

14. MONITORING AGENCY NAME & ADDRESS (if different from Controlling Office)

(12) 88 p. (11) Jan 79

15. SECURITY CLASS. (of this report): Unclassified

15a. DECLASSIFICATION DOWNGRADING SCHEDULE

16. DISTRIBUTION STATEMENT (of this Report)

Approved for public release; distribution unlimited

17. DISTRIBUTION STATEMENT (of the abstract entered in Block 20, if different from Report)

(9) Interim rept. 15 Oct 77-15 Oct 78,

18. SUPPLEMENTARY NOTES

19. KEY WORDS (Continue on reverse side if necessary and identify by block number)

Epoxy resins
Crosslink density distribution
Network inhomogeneities
Small angle x-ray scattering
Wide angle x-ray scattering

20. ABSTRACT (Continue on reverse side if necessary and identify by block number)

Considerable evidence has been accumulated by different investigators which demonstrates that the crosslink density in cured epoxy resins is not uniform. The non-uniformity of the network density can be so pronounced that the system approaches a two-phase system being composed

DD FORM 1 JAN 73 1473 EDITION OF 1 NOV 65 IS OBSOLETE

SECURITY CLASSIFICATION OF THIS PAGE (When Data Entered)

304 400

(continuation of block 20)

of a large number of densely crosslinked domains of globular shape (nodules or network clusters) which are imbedded in a common matrix of lower crosslink density.

Most of the evidence for nodule formation in cured epoxy resins is derived from electron microscopic investigations of fracture surfaces by replication technique. Generally, the micrographs reveal the presence of globular domains with dimensions in the range of 10-70 nm. So far the existence of nodular structures could not be confirmed by x-ray scattering experiments. In view of the accumulated evidence for the presence of globular network inhomogeneities the lack of x-ray evidence would indicate an extremely small difference between the electron densities of nodules and imbedding matrix material. As a consequence the evaluation of x-ray particle scattering becomes experimentally rather demanding.

During the report period small angle x-ray scattering techniques were developed to investigate and characterize cured epoxy resins for network inhomogeneities. Samples of epoxy resins were formulated and cured in series that would be expected to follow trends in size of highly crosslinked nodules according to results and theories reported in the literature. Examination of two such series of samples showed that the expected trends were followed and that the differing sizes of nodules do cause clearly discernible changes in the small angle x-ray scattering pattern. However, the need for x-ray scattering data at higher resolution is clearly indicated to allow complete interpretation. Such data are now being obtained.

FOREWORD

The project is carried out under the direction of Dr. A. Schindler, principal investigator and Dr. N. Morosoff, co-principal investigator. Dr. Schindler is responsible for overall coordination of the program and synthesis of cured epoxy resins, Dr. Morosoff for obtaining and interpreting the x-ray scattering data. Other participants were Martin Alsup responsible for day-to-day operation of the x-ray equipment and treatment of x-ray data, Gregory Whitaker who aided in preparation of cured epoxy resins, synthesis of intermediates and in obtaining and treating x-ray scattering data and Joyce Pusel who aided in the synthesis of heavy atom intermediates.

Dr. W. R. Krigbaum, Chairman, Department of Chemistry, Duke University, Durham, North Carolina, acted as consultant on x-ray investigations. The authors wish to express their appreciation for his assistance during the course of investigations.

The Project Engineer was Mr. Freeman F. Bentley of the Air Force Materials Laboratory and his helpful discussions are gratefully acknowledged.

Table of Contents

Table of Contents (Continued)

Table of Contents (Continued)

LSIT OF ILLUSTRATIONS

LIST OF ILLUSTRATIONS (Continued)

LIST OF TABLES

1.0 Summary

Small angle x-ray scattering (SAXS) and (WAXS) techniques are being developed to investigate and characterize cured epoxy resin inhomogeneities on the one hand and to elucidate the spatial distribution of crosslinks on the other. Priority was given to the first problems, i.e., network inhomogeneities.

Samples of cured epoxy resin have been formulated in series that would be expected to follow trends in size of highly cross-linked clusters according to results and theories in the literature. Examination of two such series of samples by SAXS shows that the expected trends are followed and that the differing sizes of clusters do cause clearly discernible changes in the SAXS pattern. However, the need for SAXS data at higher resolution is clearly indicated to allow complete interpretation. Such data is now being obtained.

The proposed preparation of cured epoxy resins in which heavy atoms would be present only at cross-links is described. Progress in the synthesis of the required heavy atom reagents is reported.

2.0 Introduction

2.1 Objective

The principle objective of this program is the development of methods based on x-ray scattering techniques which permit to address crosslink density distributions in cured epoxy resins.

2.2 Scope of Work

The objective of the program involves two separate problems which require different approaches. The first problem concerns the dimensional characterization of network inhomogeneities and the correlation of the degree of inhomogeneity with resin formulation and curing conditions. The second problem concerns the elucidation of the spatial distribution of crosslinks. Further work would then permit to correlate the established crosslink density distributions with physical properties of the cured resin. Both problems are being addressed by utilizing wide angle (WAXS) and small angle (SAXS) x-ray scattering techniques.

During the report period priority was given to the first problem, the investigation and characterization of network inhomogeneities. This selection was made because of the general importance of this problem as manifested by a number of recent publications dealing with nodule formation in cured epoxy resins.

3.0 Problem Definition and Approach

3.1 Network Inhomogeneities

3.1.1 Background

Considerable evidence has been accumulated by different investigators which demonstrates that the crosslink density in highly crosslinked polymeric networks is not uniform. The non-uniformity of the network density can be so pronounced that the system approaches a two-phase system being composed of a large number of densely crosslinked domains of globular shape (nodules or network clusters) which are imbedded in a common matrix of lower crosslink density. Indeed, Funke (1) states in a discussion of reaction mechanisms leading to the formation of crosslinked systems that the formation of homogeneous networks represents an exception in crosslinking polymerization.

Funke (1,2) summarizes several factors which can be responsible for the formation of network inhomogeneities in crosslinking polymerizations.

1. Difference between the reactivities of different functional groups which results in a uneven distribution of crosslinks.
2. Phase separation (microsyneresis) due to thermodynamic instability of the system.
3. Phase separation due to steric hindrance
4. Intramolecular cyclization reactions
5. Unreacted functional groups.

The importance of individual factors depends on the system under consideration, but generally, all of the factors can play a decisive role in the curing process of epoxy resins.

Uneven distribution of crosslinks caused by differences between the reactivities of different functional groups will be affected by the

chemical structures of the components of the resin formulation (e.g., monoepoxides vs. diepoxides, primary vs. secondary amines, ether vs. ester formations in anhydride cures, etc.).

Microsyneresis is a consequence of partial segregation occurring in a system on approaching its limit of thermodynamic stability. It will be mainly of importance in systems containing unreactive diluents. As shown by Dusek (3,4) a network formed in the presence of a solvent can accommodate only an amount of the latter corresponding to its swelling equilibrium value. With increasing crosslinking density the degree of swelling of the network decreases and phase separation will occur which may be enhanced by incompatibility between solvent and polymer. Microsyneresis will be affected by reaction temperature and ultimate crosslink density, as well as solubility parameters of solvent and polymer.

The occurrence of microsyneresis is not restricted to systems containing an unreactive diluent but can take place in any system in which limited compatibility between network and monomeric resin exists. Indeed, a limited compatability between network and uncrosslinked resin is assumed by several authors to explain the formation of network inhomogeneities.

Phase separation due to steric hindrance can be caused by two effects (5). Firstly, already at moderate degrees of crosslinking, residual functional groups can become separated too far to undergo further reaction. Secondly, with increasing degree of crosslinking the glass transition temperature of the polymer increases due to increasing immobilization of network segments. Consequently, as soon as the glass transition temperature approaches the curing temperature further curing reactions cease. By increasing the curing temperature renewed segmental mobility is obtained and further curing takes place (6).

A relatively low importance was assigned by Dusek et al. (7) to cyclization reactions in epoxy cures which should result in the formation of microgels. The authors claim this type of reaction to be more typical of crosslinking chain polymerizations where, at higher contents of crosslinking agent, densely crosslinked particles are already formed at the beginning of the reaction.

Contrarily to Dusek et al. (7), Lüttgert and Bonard (8) claim that the decisive factor determining the morphology of cured epoxy resins is given by the number of microgel particles formed during the very early stages of the curing process. According to these authors the onset of crosslinking occurs localized with the formation of microgel particles of high crosslink density. As the curing process proceeds, these gel particles grow in size in the liquid resin until they meet and the bulk of the material gels. Consequently, the final size of globular domains in the cured resin depends on the ratio of two rates, the rate of microgel formation (nucleation) and the rate of growth of the gel particles. At high curing temperatures the rate of nucleation will be fast and the great number of microgels formed permits growth only to a small size. Low curing temperatures initiate only a small number of gel particles and the cured resin will show large globular inhomogeneities. The proposed curing mechanism is based on results obtained from electron microscopic investigations of fracture surfaces of resins cured at different temperatures.

The existence of inhomogeneities in highly crosslinked polymer networks, especially cured epoxy resins, is supported by a wide range of experimental evidence. Swelling experiments (9, 10) indicated differences between the rates of solvent uptake for globules and matrix mater-

ial. Mechanical properties, such as tensile strength, showed large discrepancies between theoretical and experimental values which were interpreted by assuming network inhomogeneities (11).

Most of the evidence is derived from electron microscopic investigations of fracture surfaces by replication technique (7,8,12-19). Generally, the micrographs reveal the presence of globular domains with dimensions in the range of 10-70 nm. Since the presence of nodules was also observed with other polymeric networks besides epoxy resins (20-23), nodule formation can be considered as characteristic for crosslinking polymerization reactions. Micrographs of fracture surfaces of uncrosslinked, glassy polymers, such as polystyrene or poly(methyl methacrylate), reveal similar features but in a less pronounced way (24).

So far the existence of nodular structures in cured epoxy resins could not be confirmed by x-ray scattering experiments (7,16,17). In view of the accummulated evidence for the presence of globular network inhomogeneities the lack of x-ray evidence would indicate a very small difference between the electron densities of nodules and embedding matrix material. This conclusion is not inconsistent with the suggestion that the microscopically observed nodules represent regions of higher crosslink density, for an increase in the latter may only slightly affect the local electron density (17).

An essentially uniform electron density throughout the bulk of cured epoxy resins is also indicated by the absence of structural features in transmission electron microscopy of microtomed samples (25). Apparent regions of high crosslink density at the edge of a craze were observed by transmission electron microscopy of an amine cured epoxy resin (26), but the large dimensions of these regions (200-1000 nm) are

far outside the range of nodule dimensions generally observed on fracture surfaces.

3.1.2 Small Angle X-Ray Scattering

A detailed discussion of SAXS as applied in the morphological investigations of cured epoxy resins will be given in a later section. In this section only some principles are discussed which affect sample selections and preparations.

For the purpose of our investigations a cured epoxy resin possessing an inhomogeneous network structure (nodules) may be considered to correspond in its x-ray scattering effects to a system composed of low molecular weight solvent in which particles of colloidal dimensions are dispersed. The colloidal particles of the model system would correspond to the densely crosslinked nodules whereas the solvent corresponds to the matrix of uniform low crosslink density. In such a system the total SAXS effect is composed of three contributions (27).

(a) The scattering of the solvent (matrix) which is generally very weak in the small angle region. (b) The actual particle scattering which can be observed only if a sufficient difference in electron densities exists between particles (nodules) and solvent (matrix). The intensity of the scattered radiation generally increases with decreasing scattering angle. From the shape of the intensity distribution close to the primary beam conclusions can be derived with respect to shape and size of the scattering particles. (c) Density fluctuation inside the particles cause a constant background intensity in the small angle region.

The intensity of the particle scattering depends on the magnitude of the electron density difference between both phases. This difference

is rather small in cured epoxy resins. Dusek et al. (7) estimated a value not exceeding 0.005 mol/cm^3, i.e., the difference between the densities of nodules and matrix would be smaller than 0.01 g/cm^3. Because of this small density difference the intensity of sample scattering deviates only slightly from the background intensity resulting from instrumental scattering.

Initially, it was intended to investigate epoxy resins cured with hardeners containing heavy atoms of high x-ray scattering power (e.g., chlorine, bromine, tin). This approach was abandoned since an increase in the electron density difference between nodules and matrix cannot be achieved by this method. It seems reasonable to assume that the difference in crosslink densities between nodules and matrix will not be affected to a large extent by the kind of hardener used. Since the difference in crosslink densities determines the difference in electron densities an increase in contrast between nodules and matrix will not be achieved with the use of labeled hardeners.

Labeled hardeners of high x-ray scattering power would be useful in the present study only if they were selectively distributed between the two phases of the cured resins. Such a possibility might be realized by using a combination of labeled and unlabeled hardeners of strongly differing reactivities in the curing process. If one assumes the nucleation theory of Lüttgert and Bonart (8) to apply, the more reactive hardener should preferentially participate in the initial formation of the microgel particles. Such a system would be given by dichloromaleic anhydride and maleic anhydride where the former compound cures considerably faster than the latter. As a consequence the core of the nodules should have a higher chlorine concentration than the matrix and the particle scattering power of the resin should be increased.

Although the outlined resin preparation might result in improved particle scattering, the interpretation of SAXS data of such samples cannot be generalized due to the complexity of the curing system. The electron density difference between nodules and matrix can be increased in resins cured with conventional hardeners by utilizing the effect of crosslink density on the swelling properties of crosslinked networks. The solvent uptake by the less densely crosslinked matrix will be higher than by the more densely crosslinked nodules. Consequently, the use of a swelling agent of high electron density, such as brominated aliphatic or aromatic hydrocarbons, will generate the desired electron density difference and increase the particle scattering of the sample.

Since the required contrast between nodules and matrix cannot be achieved with labeled hardeners unlabeled hardeners were used in most of our resin preparations. The use of conventional hardeners has the advantage that resin formulations and curing conditions can be investigated which are close or even identical to those applied in practical applications.

Labeled hardeners, especially brominated anhydrides, also present experimental problems in sample preparations. The high molecular weights of the hardeners require resin formulations which often exceed the solubility limit of the hardener in the epoxy resin. This unfavorable situation is aggravated by the high melting points of brominated anhydrides which require elevated casting temperatures with the possibility of premature gelling of the resin.

The extremely small electron density difference between nodules and matrix of conventionally cured epoxy resins required the development of a sophisticated experimental technique for our SAXS investigations. For

this purpose conditions of sample preparation were selected which could be anticipated to yield networks possessing different degress of inhomogeneity.

Resin samples so far investigated by SAXS technique are all derived from a triepoxide (Ciba-Geigy PT-810) cured with anhydrides. In anhydride cures, both the epoxy group and the anhydride group act difunctional. Consequently, a tri-epoxide has a maximum functionality of six at a compositional ratio of one anhydride group per epoxy group. By decreasing this ratio to a value of 0.67 the triepoxide will have an average functionality of four and correspond in its curing behavior to a diepoxide. One can expect that resins cured at different epoxy to anhydride ratios will differ with respect to extent and dimensions of network inhomogeneities. Especially at low anhydride concentrations the formation of densely crosslinked nodules might be anticipated since during the early stage of the curing process part of the tri-epoxide will exert is maximum functionality due to the initial abundance of anhydride.

Further changes in network morphology were affected by using resin formulations containing varying amounts of an unreactive diluent (dimethylphthalate) and by performing the curing process at different temperatures.

3.2 Crosslink Density Distribution

The elucidation of the crosslink density distribution in cured epoxy resins has already been addressed in part by the evaluation of the observed intensity distribution caused by particle scattering in SAXS experiments. These experiments reveal the presence of domains with crosslink density exceeding that of the surrounding material and thus

demonstrate for such resins a biomodal form of the overall crosslink density distribution.

Experimental determinations of distances between crosslinks in polymeric networks were performed recently with model networks utilizing SAXS (28,29) and neutron coherent scattering (29,30) techniques. The model networks for SAXS were prepared by anionic polymerizations which yielded monodisperse chain segments of predetermined lengths which could be connected by ironlabeled crosslinks during network formation. SAXS by these network revealed the presence of one single but rather broad diffraction band. For a given network the position of the band maximum was found to be a function of the degree of swelling of the gel. For a series of networks differing merely in the average segment length between crosslinks the maximum shifted to lower scattering angles as the average segment length increased.

It followed from these SAXS results that a well-defined correlation distance exists between first neighbor crosslinks. There is, however, no correlation between the position of second neighbor crosslinks: the network behaves in this respect as amorphous compounds or as liquids (29).

The application to cured epoxy resins of the outlined SAXS technique for structural investigations of model networks requires some further considerations. The most pronounced difference between both kinds of networks is given by the extremely high crosslink density in epoxy resins.

In the model networks the observed Bragg spacings corresponding to the average distances between crosslinks varied between 10 and 20 nm. These values are about one order of magnitude larger than can be estimated

for crosslink distances in cured epoxy resins which have to correspond to the molecular dimension of one epoxy-hardener pair. As a consequence, the positions of the intensity maximum in the diffractogram representing the average Bragg distance of crosslinks will occur in the wide angle region and will coincide with intensity maxima caused by general short range intra- and intermolecular ordering in the network. The latter maxima were found by Dusek et al. (7) to correspond to Bragg distances of about 0.5 and 1.5 nm in a resin derived from the diglycidyl ether of bisphenol-A.

In principle, the strong overlap or near coincidence of both, the amorphous scattering of the resin and the scattering due to the labeled crosslinks, can be resolved by subtracting the scattering curves of two resins prepared under identical conditions but possessing labeled and unlabeled crosslinks, respectively. The method will be subjected to some inaccuracy since short range ordering in both samples will differ to some extent due to the presence and absence of the labeling atoms. Furthermore, the evaluation of the scattering curves will be affected by any difference between both samples concerning the extent of network inhomogeneities. For this reason the elucidation of particle scattering was assigned priority in our work in order to characterize film samples prior to further detailed investigations.

According to the synthetic method used for the preparation of model networks, the functionalities of the iron labeled centers varied to some extent but it could be assumed that each center will have a functionality exceeding a value of two, i.e., each labeled center will represent a crosslink in the network. This necessary condition for the elucidation of crosslink densities by x-ray scattering techniques is not met by epoxy resins containing labeled crosslinks.

In order to simplify the discussion, only network formations will be considered which occur between difunctional and tetrafunctional components. Such network formations are represented by cures of diepoxides with either anhydrides of dicarboxylic acids or primary diamines.

Anhydride cures in the absence of catalyst require the presence of hydroxyl groups in the epoxy resin, e.g., secondary hydroxyls found in the higher molecular weight epoxides based on bisphenol-A. According to Fisch et al. 6,31) the anhydride ring is opened by the hydroxyl group under formation of a half-ester, eq. (1a). The half-ester then reacts through its acid group with a second epoxy ring thereby forming a hydroxy diester, eq. (1b). The hydroxyl group of the diester can be consumed either in further esterification reactions with anhydride groups or can undergo etherifications reactions with epoxide groups, eq. (1c).

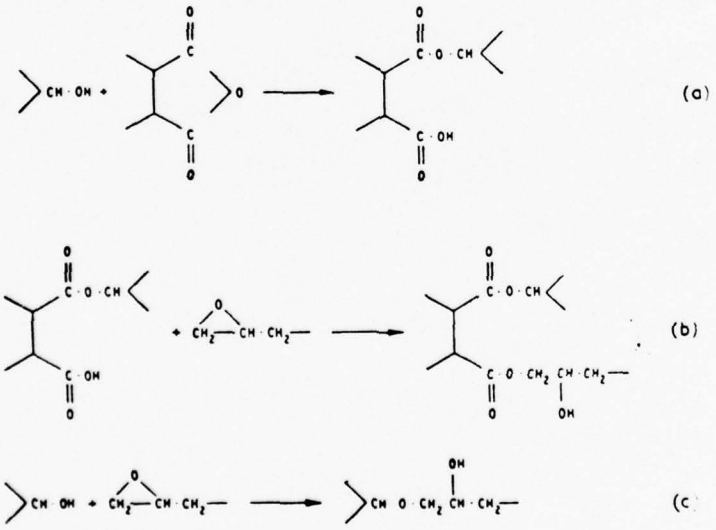

(a)

(b)

(c)

Undesirable etherification reactions can be suppressed by tertiary amine catalysis of the curing process. Tanaka and Kakiuchi (32) concluded

from their kinetic analysis of base-catalyzed curing processes that etherification did not occur below 140°C. The reaction sequence for tertiary amine catalyzed cures as suggested by Fischer (33) involves the alternating formation of alkoxide esters and carboxylate ions.

carboxylate ion + epoxide ring → alkoxide ester

alkoxide ester + anhydride → carboxylate ion

as shown in eq. (2).

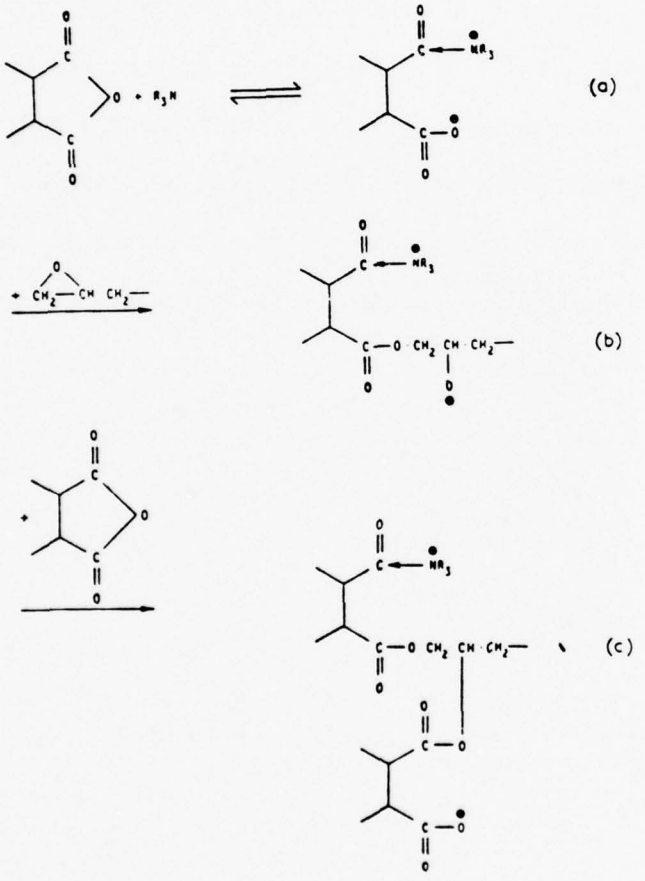

(2)

Provided one uses well defined epoxy resins free of hydroxyl groups and pure anhydrides free of carboxyl groups, curing will not occur even

at elevated temperatures prior to the addition of the amine catalyst. This is of special importance for the formulation of high melting epoxides and anhydrides.

In amine cures the functionalities of hardener and resin are reversed with respect to anhydride cures, the primary diamine being tetrafunctional and the diepoxide being difunctional. At stoichiometrically equivalent ratios of functional groups or in the presence of excess amine, the consecutive reaction of the epoxide groups with the hydrogen atoms of the amino groups is the only reaction taking place (34).

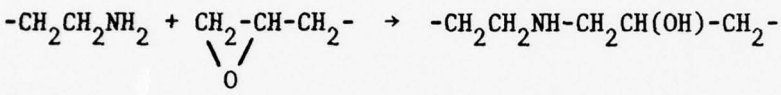

(3a)

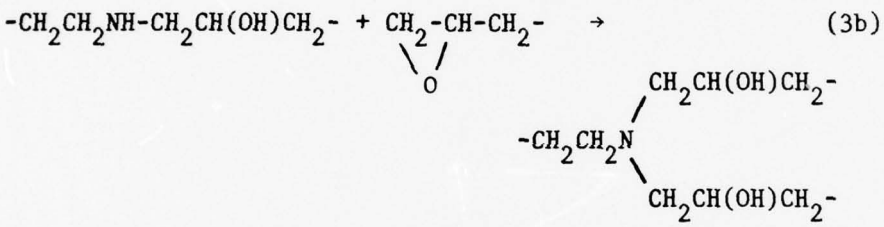

(3b)

If epoxide groups are present in excess, the hydroxyl groups formed in the reaction can participate in the formation of ether linkages (34).

With both curing mechanisms, anhydride and amine cure, networks of maximum crosslink density should result under ideal conditions if tetra and difunctional components are used in stoichiometric ratio and if the tetrafunctional component fully exercises its functionality. From a structural point of view these networks are identical for both curing mechanisms. A two-dimensional representation of such an ideal network is shown in Figure 1 where tetra and difunctional components are designated by rectangles and circles, respectively.

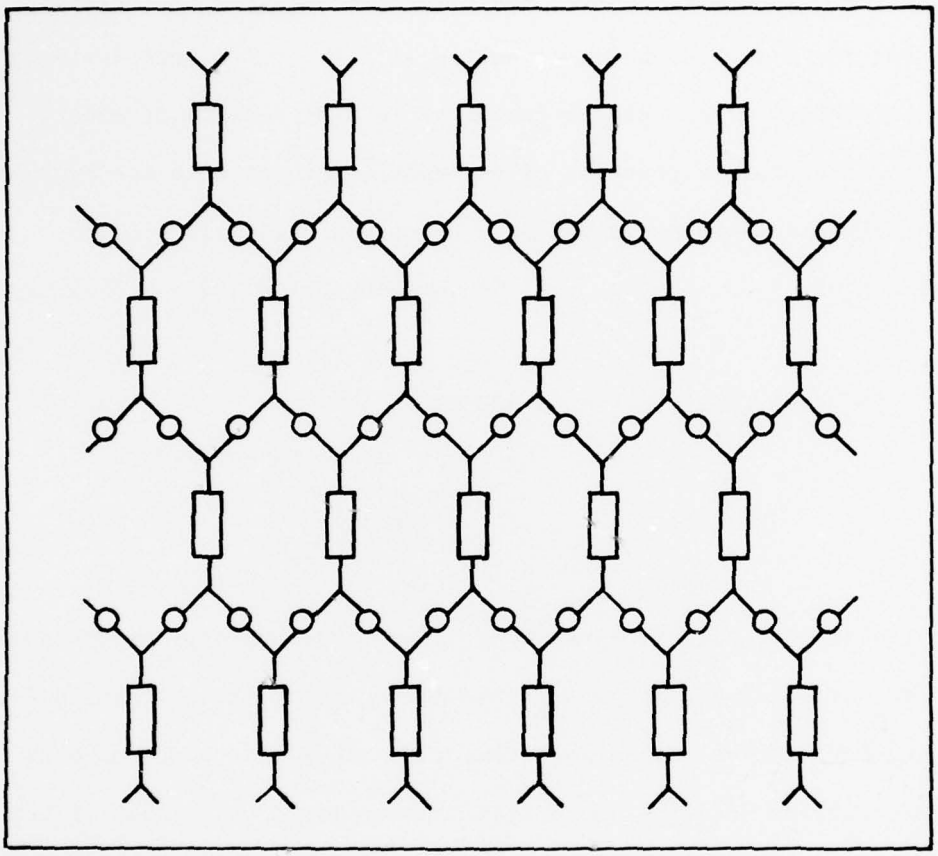

Figure 1. Schematic representation of an ideal network derived from tetrafunctional (rectangles) and difunctional (circles) components in stoichiometric ratio.

The actual crosslinks as defined by the branching points of the chains have different chemical structures depending on the curing mechanisms. In anhydride cures one obtains

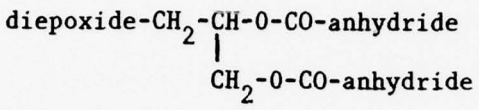

whereas primary diamine cures yield

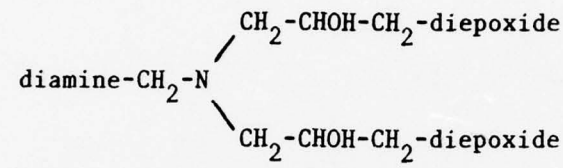

It is obvious that the branch point cannot be labeled for x-ray work but only some part of the molecule of the tetrafunctional component. This means the network is labeled by the rectangles in the schematic presentation of Figure 1.

Actual network structures of cured epoxy resins will deviate considerably from the idealized structure of Figure 1. These deviations will be a consequence of not all of the functionalities of both components being fully exercised. Because of its high irregularity such a network is difficult to depict in a two-dimensional representation, especially concerning the spatial distributions of the tetrafunctional component.

In Figure 2 two network irregularities are schematically indicated where one tetrafunctional moiety, depicted as a solid rectangle, acts only difunctional. In the schematic network of Figure 3, two tetrafunctional molecules act only trifunctional. In both cases the mesh size of the network is increased by the incomplete reaction of the tetrafunctional component, i.e., the crosslink density is decreased. Incomplete reactions of the tetrafunctional components with concomitant

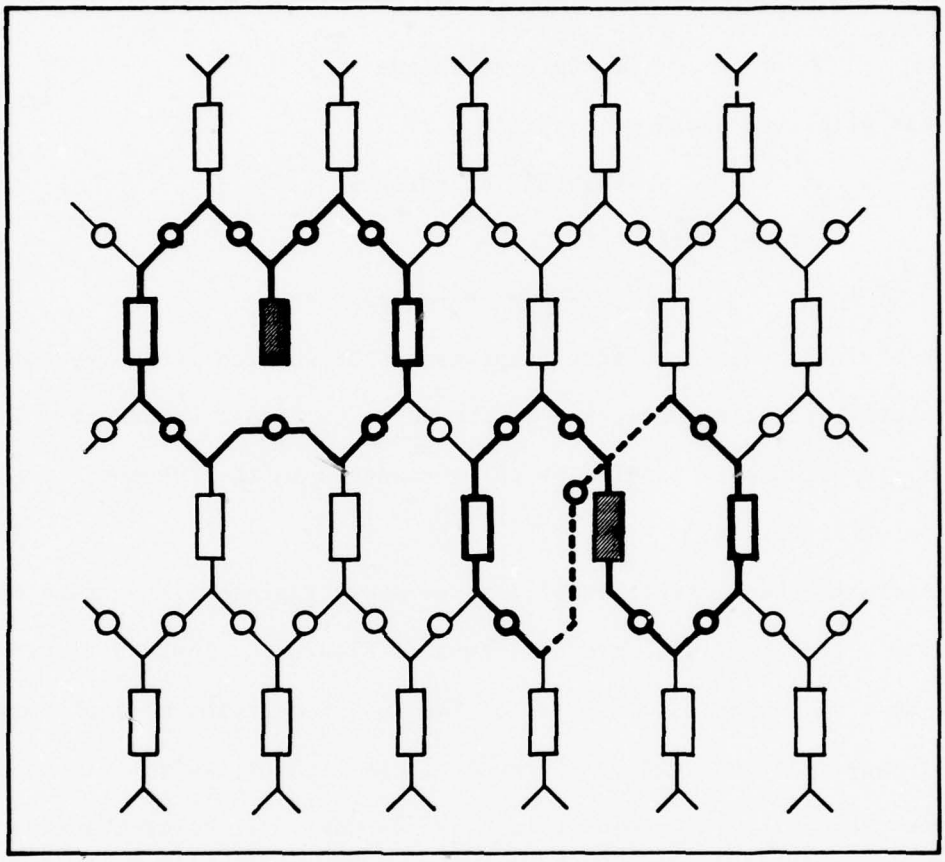

Figure 2. Schematic representation of a network derived from tetrafunctional (rectangles) and difunctional (circles) components with some of the tetrafunctional components exercising a functionality of two.

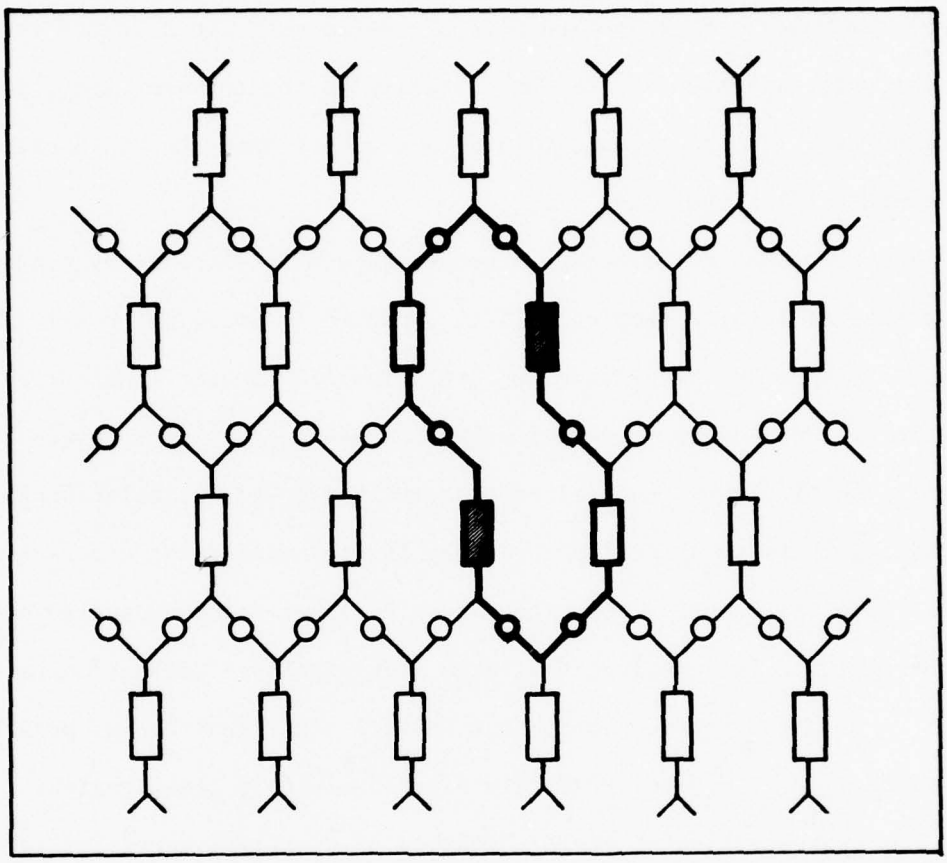

Figure 3. Schematic representation of a network derived from tetrafunctional (rectangles) and difunctional (circles) components with two of the tetrafunctional molecules exercising a functionality of three.

changes in crosslink densities will have only a minor effect on the x-ray scattering properties of samples prepared with labeled tetrafunctional compounds. Each labeled molecule would contribute to the scattered intensity irrespective of its functionality in the network, i.e., participation of a labeled component in either crosslinking or chain extension could not be distinguished.

The effect of differences in crosslink densities on x-ray scattering properties of labeled samples will be enhanced by swelling in solvents of low electron density. The lower the crosslink density the more the network will expand thereby increasing the average distance between chains. In highly swollen regions the intermolecular correlation between scattering centers may be lost and only the intramolecular correlation will remain representing the alternation of labeled and unlabeled moieties in the chains. In densely crosslinked (less swollen) regions intramolecular correlation between scattering centers might persist and permit the estimation of crosslink density distributions in these regions.

The basic problem in the elucidation of crosslink densities in cured epoxy resins is given by the fact that changes in crosslink density are solely caused by the polyfunctional compound not exercising its maximum functionality. Since irrespective of the degree of functionality exercised, polyfunctional and difunctional components alternate in the network chains crosslinks cannot be distinguished from chain extension by labeling the polyfunctional component with centers of high x-ray scattering power. Indeed, for the suggested x-ray investigations on swollen films it is irrelevant whether the polyfunctional or the difunctional component has been labeled with heavy atoms.

The interpretation of x-ray scattering results would be greatly simplified with systems in which the scattering centers are exclusively inserted at the crosslinks. Appropriate systems approaching this condition would be given by resin formulations containing reactive diluent (chain extenders) such as mono and diepoxide for anhydride cures with the diepoxide being labeled. Correspondingly, in amine cures of diepoxides one would have to use secondary diamine in combination with labeled primary diamine (11).

The curing mechanism of such systems strongly resembles the crosslinking mechanism in free radical polymerization of mono and divinyl compounds. In the latter mechanism crosslink density and crosslink density distribution are determined by the copolymerization behavior of both components, i.e., by the values of their respective copolymerization parameters. This applies also for the curing mechanism of epoxy systems. In anhydride cures the reactivities of mono and diepoxide toward the anhydride will be different and copolymerization parameters can be assigned to both components thus permitting to describe the system by the usual copolymerization equation. The more reactive component will be consumed faster and the crosslink density will change to some extent as the curing process proceeds. Analogous considerations apply to amine cures with the secondary diamine corresponding to the monoepoxide in anhydride cures and the primary diamine corresponding to the diepoxide.

By varying the proportions of difunctional diluent in the resin formulations, networks can be prepared differing in their crosslink densities. The range of crosslink densities can be extended from weakly crosslinked systems for which rubber elasticity theory still applies to densely crosslinked systems for which the theory fails. On these systems

crosslink density distributions should be accessible by x-ray scattering techniques provided the distribution of crosslink distances is not too broad.

4.0 Preparation of Cured Resin Samples

4.1 Curing Procedure

X-ray scattering experiments require only small samples of 1 x 4 cm in size. The thickness of the samples should be uniform and should not exceed an optimum value depending on the chemical composition of the resin which determines its x-ray absorbance. The latter condition is only of importance for samples containing heavy atoms, samples prepared with conventional resins formulations were generally made of thickness below the optimum value to allow for uptake of brominated solvents in swelling studies. Differences in sample thicknesses are not critical since our SAXS intensities are normalized for the same primary beam intensity.

The formulated resins are cured between glass plates using thin Silastic or Teflon tubings as gaskets. During the initial part of our studies severe problems were encountered with the release of the cured samples from the plates. This problem has been solved by proper plate treatment.

Clean glass plates are evenly sprayed with Frekote 34 (Frekote, Inc., Boca Rota, Fla.) and air dryed. The plates are then baked for 5-6 hrs at 230-250°C in a glass annealing oven. After cooling to ambient temperature the plates are ready for one-time use. For reuse the plates have to be cleaned and recoated since some of the Frekote coating is transferred to the resin surface as indicated by its hazy appearance.

Epoxy resin and anhydride are weighed in a glove bag under nitrogen to prevent access of humidity. Screw cap vials of 20 ml capacity are used. Depending on the melting points of epoxide and anhydride, the closed vials are sufficiently heated with an air gun to obtain a homo-

genous blend which is then degassed in a vacuum oven set at proper temperature to keep the resin viscosity sufficiently lower. After degassing tertiary amine accelerator (dimethyl benzylamine) is added via a microsyringe and carefully blended without reintroducing air bubbles.

The blended resin is cast on a prepared glass plate at the center of a Silastic ring. The mold is closed with a second plate and is secured with binder clips. Formulations with high melting epoxides or anhydrides require preheated plates to prevent recrystallization of the compounds.

Curing is performed by placing the plates upright in a thermostated circulating air oven. After the required curing period the molds are slowly cooled to ambient temperature and pried open.

It was found that cured epoxy resins possessing optically clear surfaces can be obtained by curing between glass plates on which fluorinated polymers had been deposited by plasma polymerization. Especially a coating resulting from plasma deposition of perfluorodibutyl tetrahydrofuran could be reused repeatedly without deterioration of its release property. Since our equipment for plasma deposition presently permits only coating of microscopy slides, Frekote coated glass plates of larger dimensions were used for sample preparation.

4.2 Resin Formulations

In order to test the applicability of SAXS techniques for the elucidation of network morphologies, resin formulations and curing conditions were selected for which large variations in the extent of network inhomogeneities could be anticipated. A triepoxide, PT-810 (Ciba-Geigy) was considered most appropriate for this purpose and a

considerable number of samples was prepared under varying conditions listed in Table I and II.

The triepoxide of structural formula

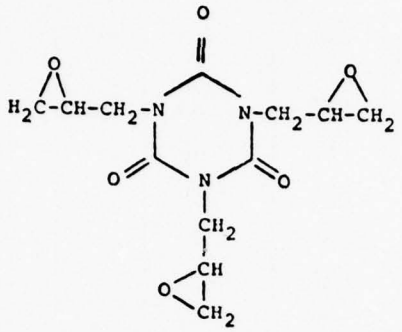

is a relatively well defined compound with a narrow melting range around 125°C. The reported molecular weight per epoxy group is in the range of 102-109 in fair agreement with the theoretical value of 99.

In Table I are summarized resin preparations in which varying amounts of unreactive diluents were used. These experiments were designed to observe possible effects of microsyneresis on nodule formation in the resins. The diluents were selected for high boiling points and for solubility parameters in the range of 10-11 $cal^{1/2}/cm^{3/2}$ (0.0205-0.0226 $J^{1/2}/m^{3/2}$) to assure initial compatibility with the resin. The diluents were

Diluent	Boiling Point (°C)	Solubility Parameter ($cal^{1/2}/cm^{3/2}$)
Dibutylphthalate (DBP)	340	9.9
Dimethylphthalate (DMP)	283	11.0
Tetrabromoethane (TBE)	240	10.3

With bis(2-methoxyethyl)ether (bp=162°C) it was not possible to obtain bubble-free samples in 140°C cures. Tetrabromoethane was used as

Table I. Epoxy resins prepared from a triepoxide (Ciba-Geigy PT-810) by anhydride cure in the presence of unreactive diluents.

Sample Designation	Anhydride		Diluent		Hours Cured At		
	Kind	R_H	Kind	ml/g	80°C	120°C	140°C
D-1	THPA	0.9	DMP	0.88	-	15	-
D-2	THPA	0.9	DMP	0.44	-	15	-
D-3	THPA	0.9	DMP	0.22	-	15	-
K-1	DCMA	0.9	DMP	1.00	-	19	-
K-2	DCMA	0.9	DMP	1.00	3	14	-
K-3	DCMA	0.6	DMP	0.88	-	16	-
K-4	DCMA	0.6	DMP	0.88	2	14	-
K-5	DCMA	0.9	DMP	1.00	2	14	-
L-1	DBTHPA	0.9	DMP	0.54	93	6	-
L-2	DBTHPA	0.6	DMP	0.54	93	6	-
M-1	DBTHPA	0.9	DBP	0.54	16	-	-
M-2	DBTHPA	0.9	DBP	0.54	16	-	-
N-1	DBTHPA	0.9	DMP	0.54	25	-	-
N-2	DBTHPA	0.9	DMP	0.54	17	4	4
N-3	DBTHPA	0.9	DMP	0.54	17	8	-
R-1	NMA	0.6	TBE	0.03	24	-	-
R-2	NMA	0.6	TBE	0.07	24	-	-
R-3	NMA	0.6	TBE	0.03	16	8	-
R-4	NMA	0.6	TBE	0.07	16	8	-
R-5	NMA	0.6	TBE	0.03	16	4	4
R-6	NMA	0.6	TBE	0.07	16	4	4

Anhydrides: THPA = Tetrahydrophthalic anhydride
DCMA = Dichloromaleic anhydride
DBTHPA = Dibromotetrahydrophthalic anhydride
NMA = Nadic methyl anhydride

R_H = mol anhydride/mol epoxy group

Diluents: DMP = Dimethyl phthalate
DBP = Dibutyl phthalate
TBE = Tetrabromo ethane

a labeled diluent in order to observe the possible formation of solvent clusters in the cured resin.

In Table II are summarized curing conditions for resins prepared from PT-810 triepoxide in the absence of diluents. In these preparations different curing temperatures were used to affect network morphology. This approach would be in accordance with the nucleation theory of Lüttgert and Bonart (8) discussed previously.

All sample preparations based on PT-810 were made by anhydride cures including unlabeled (tetrahydrophthalic anhydride and methyl nadic anhydride) and labeled anhydrides (dichloromaleic anhydride and dibromo-tetrahydrophthalic anhydride). Two molar ratios of anhydride to epoxy groups, R_H = 0.9 and 0.6, were applied. At the higher ratio the amount of anhydride nearly suffices for the triepoxide to fully exercise its functionality. At the lower ratio the average functionality of the triepoxide will be four. Also in this case highly crosslinked networks result but with enhanced probability for the formation of inhomogeneities.

Several samples were prepared from Epon 828 cured with diethylene tetramine and from Epon 812 cured with methyl nadic anhydride. Resin formulations and curing conditions corresponded to those reported by Racich and Koutsky (17) in their studies of fracture surfaces. Since the authors claimed good reproducibility of nodule formation, such samples were considered as appropriate test material for SAXS investigations.

4.3 Labeled Resin Components

Heavy atoms for providing centers of high x-ray scattering power in the cured resin are more easily introduced into the hardeners than into the epoxide. For this reason a brominated anhydride and a tin containing diamine were selected for our investigations.

Table II. Epoxy resins prepared from a triepoxide (Ciba-Geigy PT-810) by anhydride cures at different temperatures.

Sample Designation	Anhydride		Hours Cured At				
	Kind	R_H	80°C	120°C	130°C	140°C	180°C
D-4	THPA	0.9	-	4	-	-	-
P-1	NMA	0.9	25	-	-	-	-
P-2	NMA	0.9	17	8	-	-	-
P-3	NMA	0.9	17	4	-	4	-
P-4	NMA	0.6	25	-	-	-	-
Q-1	NMA	0.9	26	-	-	-	-
Q-2	NMA	0.9	18	8	-	-	-
Q-3	NMA	0.9	18	4	-	4	-
Q-4	NMA	0.6	26	-	-	-	-
Q-5	NMA	0.6	18	8	-	-	-
Q-6	NMA	0.6	18	4	-	4	-
Q-7	NMA	0.9	-	-	16	-	-
Q-8	NMA	0.9	-	-	-	-	6

Anhydrides: THPA = Tetrahydrophthalic anhydride
NMA = Nadic methyl anhydride

R_H = mol anhydride/mol epoxy group

Bromine containing anhydrides are commercially available in the form of tetrabromophthalic anhydride and bromomaleic anhydride, but both components were not usable for resin preparations. Because of the high molecular weight of tetrabromophthalic anhydride (MW=464) resin formulations require weight ratios of anhydride to epoxide which exceeded by far the solubility of the anhydride in the epoxide. Blending of both components at elevated temperatures fails due to the high melting point of the anhydride at 275°C. Bromomaleic anhydride is liquid at ambient temperature and can be conveniently blended with epoxides. Unfortunately, the compound was found to develop acidic fumes during curing due to insufficient temperature stability.

A suitable bromine containing anhydride, dibromotetrahydrophthalic anhydride (DBTHPA), was prepared by bromination of tetrahydrophthalic anhydride (THPA) in chloroform (36,37). THPA, recrystallized from toluene, was dissolved in chloroform and a solution of bromine in chloroform was added dropwise under stirring at room temperature until a faint bromine color prevailed for several hours. The precipitated DBTHPA was filtered, washed several times with hexane, and dried. The compound melted at 136-137°C (36). Percent bromine contents determined on three batches (Galbraith Laboratories, Knoxville, Tennessee) were 51.10, 51,05 and 50.93% versus a theoretical value of 51.24%.

Resin formulations containing DBTHPA require handling at elevated temperature (100-110°C) to prevent crystallization of the anhydride. At these temperatures the pot life of the resin is rather short, especially after addition of the tertiary amine catalyst. Unreactive diluents were used to increase anhydride solubility and to extend the pot life of the resin.

For x-ray investigations of epoxy resins prepared by amine cure, a tin containing primary diamine was selected. The compound, bis(3-aminopropyl) dibutyl tin, $(C_4H_9)_2Sn(CH_2CH_2CH_2NH_2)$ has been synthesized as a yellow and viscous oil which is difficult to purify. In a preliminary curing experiment with Epon 828 an incompletely cured film was obtained.

The synthesis of the compound, which has not been described in the literature, involves three steps: (1) reduction of dibutyltin dichloride to dibutyltin dihydride (38).

$$(n\text{-}Bu)_2SnCl_2 + LiAlH_4 \rightarrow (n\text{-}Bu)_2SnH_2$$

(2) hydrostannylation of acrylonitrile (39,40)

$$(n\text{-}Bu)_2SnH_2 + 2CH_2{=}CHCN \rightarrow (n\text{-}Bu)_2Sn(CH_2CH_2CN)_2$$

and (3) reduction of the dinitrile to the diamine (41).

$$(n\text{-}Bu)_2Sn(CH_2CH_2CN)_2 + LiAlH_4 \rightarrow (N\text{-}Bu)_2Sn(CH_2CH_2CH_2NH_2)_2$$

In several preparations the dibutyltin dihydride was obtained with 60-70% yield. The boiling point at 12 mm Hg (1.6 kPa) was 75°C as reported. The yield of dinitrile could be improved by catalyzing the hydrostannylation reaction with a free-radical initiator, azo-bis(isobutyronitrile) (40). The reaction was monitored by ^{1}H-NMR spectroscopy for the disappearance of the dihydride. After bulb-to-bulb distillation at 150°C and a pressure of 5×10^{-4} mm Hg (0.07 Pa) a clear, yellow oil was obtained in 50% yield. The ^{1}H-NMR spectrum in $CDCl_3$ exhibited the proper ratio of butyl to ethylene protons. Purification of the diamine so far was not successful.

It is intended to omit the reduction step from dinitrile to diamine by direct hydroatannylation of allylamine

$$(n\text{-}Bu)_2SnH_2 + 2CH_2{=}CHCH_2NH_2 \rightarrow (n\text{-}Bu)_2Sn(CH_2CH_2CH_2NH_2)_2$$

Product isolation from hydrostannylation reactions is considerably simpler than from the nitrile reduction with $LiAlH_4$. Hydroatannylations are carried out with excess of the olefin as solvent which can be removed by distillation (allylamine: bp = 53°C). The main product is then purified by bulb-to-bulb distillation under high vacuum.

5.0 X-Ray Scattering

5.1 Interpretation of X-Ray Scattering Data

5.1.1 Desmearing of Slit Collimated X-Ray Scattering Data

Desmearing of SAXS data obtained from a Kratky camera is required because slits, rather than pinholes, are used to collimate the x-ray beam. The intersection of the x-ray beam with the sample is therefore a line, whereas it would be a point for pinhole collimation. For an isotropic sample, as our crosslinked epoxy resins are, the intensity of scattering will be constant for any given scattering angle. If pinhole collimation is used, and the scattering intensity is registered on a piece of flat film, perpendicular to the x-ray beam, the pattern on that film will be circularly symmetric. The center will be at the intersection of the x-ray beam with the film and the darkening of the film will be constant for any given radius. If we denote the radial distance by m, and we consider that such a distance is directly related to scattering angle, the quantity we are interested in measuring is I(m), the intensity of scattering as a function of m. Now the intersection of a slit collimated beam with a film perpendicular to the beam is a line. This line may be thought of as a series of points from imaginary pinhole collimated beams strung out along the line. Each of these points will have its own circularly symmetrical scattering pattern associated with it. The patterns from adjacent imaginary pinhole beams are thus superimposed on each other. This situation is illustrated in Figure 4. In Figure 4 an x-ray beam is illustrated scattering from a sample with the scattering pattern registered on a film. The angle of scattering is denoted as 2θ. In Figure 4, the intersection of a line beam with the film is shown as a straight line. The imaginary point components of this line,

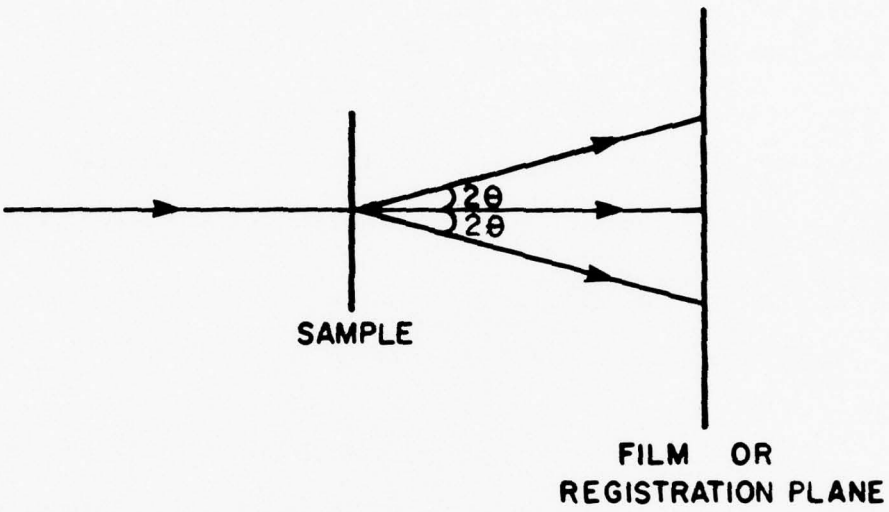

Figure 4a. Schematic representation of the x-ray scattering experiment.

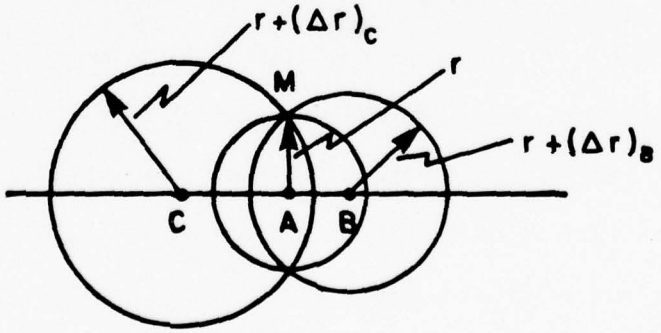

Figure 4b. Intersection of the scattered x-rays with the registration plane for a slit collimated beam. The line beam may be thought of as composed of many points, lined side by side. Three of these points are designated A, B, C. Portions of the cylindrically symmetrical scattering pattern for each point are shown intersecting at point M.

A, B, and C, are shown together with circles representing the circularly symmetric scattering associated with point A at a distance r with point B at a distance $r + \Delta r_B$ and with point C at a distance $r + \Delta r_C$. We may represent the observed intensity of scattering from the slit collimated beam as $\tilde{I}(m)$, and the scattering from each point component as $I(m)$. It is seen that the $\tilde{I}(m)$ observed at a distance m from the line contains $I_B[m + (\Delta m)_B]$, $I_C[m + (\Delta m)_C]$ as well as $I_A(m)$. $\tilde{I}(m)$ is described as being slit smeared with respect to $I(m)$. The general expression for $\tilde{I}(m)$ in terms of $I(m)$ is given as

$$\tilde{I}(m) = \int_{-\infty}^{+\infty} P(t) \; I\left(\sqrt{m^2 + t^2}\right) dt \qquad (4)$$

where $P(t)$ is a weighting function which depends on the distribution of intensity along the line shown in Figure 4. In general, the intensity distribution along the beam will be trapezoidal as shown in Figure 5. If the length of the top part of the trapezoid (representing constant intensity) exceeds the m at which $\tilde{I}(m)$ is negligible, the beam may be considered infinite, and $P(t) = 1$ in equation 4. In terms of Figure 5 an infinitely long beam is one for which $(\ell-k)>m$ for the smallest m above which $\tilde{I}(m) = 0$. It is assumed that $\tilde{I}(m)$ is measured at a point corresponding to the center of the trapezoidal distribution with a slit of infinitely small lateral extent. Since, in general, a slit of some lateral extent, 2z, is used, the condition for an infinite beam is $(\ell-k-z)>m$ for the smallest m above which $\tilde{I}(m) = 0$. We will see later that this condition may be modified slightly if the trapezoidal distribution adheres to certain conditions.

The process of obtaining the intensity distribution $I(m)$ from the observed intensity distribution $\tilde{I}(m)$ is referred to as desmearing.

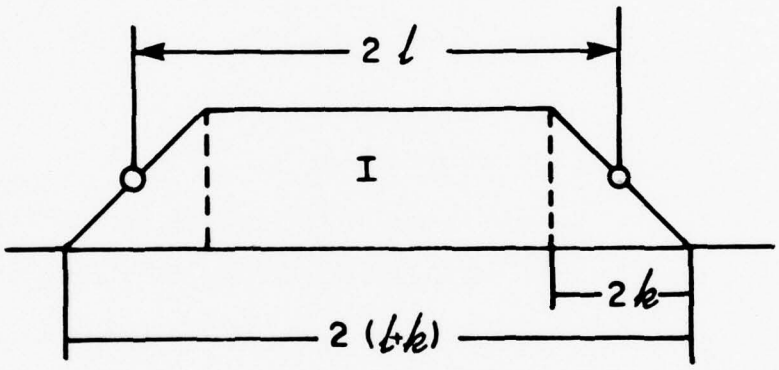

Figure 5. Typical Kratky camera incident beam profile at registration plane.

5.1.1.1 Desmearing for an Infinite Beam

For an infinite beam equation 4 may be rewritten as

$$\tilde{I}(m) = 2 \int_0^\infty I(\sqrt{m^2 + t^2})dt \qquad (5)$$

Guinier and Fournet[27,41,42] and du Mond[27,42,43] showed that this could be desmeared in the following way: The derivative of the observed intensity distribution is obtained and divided by m. This quantity is called F(m).

$$F(m) = \frac{-\tilde{I}'(m)}{m}$$

It can then be shown that I(m) is proportional to the smeared F(m), i.e., to $\tilde{F}(m)$

$$I(m) = \frac{1}{2\pi}\tilde{F}(m) = \frac{1}{\pi}\int_0^\infty F(\sqrt{m^2 + s^2})ds \qquad (7)$$

5.1.1.2 Desmearing for a Finite Beam

For a finite beam desmearing may be carried out by a modification of equation 7, provided that the intensity distribution along the beam satisfies the following criterion. The shape of the symmetrical trapezoid must be such that $k/\ell = 0.4$[27,44] (See Fig. 5). When a counter slit of finite length is used the effective trapezoidal shape is modified by the length (lateral extent) of the counter slit. If 2k of the beam profile and 2z, the length of the counter slit, are similar in magnitude with z>k, then the effective width of the shoulder of the trapezoid, $2\bar{k}$, is given as

$$2\bar{k} = 2z + 2k/3 \qquad (8)$$

If $\frac{2\bar{k}}{2\ell} = \frac{2k + 2k/3}{2\ell} = 0.4$, then the equation for desmearing becomes[27]

$$I(m) = \frac{1}{\pi}\int_0^{\ell-k} F(\sqrt{m^2 + s^2})\, ds + \frac{1}{2\ell}\tilde{I}\,(\sqrt{m^2 + (\ell-\bar{k})^2}) \qquad (9)$$

This may be recognized as a modification of equation 7. It may also be noted that when $\tilde{I}(m) = 0$ for $m > (\ell - \bar{k})$ the x-ray beam length is effectively infinite and equation 6 reduces to equation 5.

5.1.1.3 Beam Shape and Counter Slit Length and Desmearing at R.T.I.

The beam profile and counter slit length have been adjusted to satisfy the criteria given by equation 8. This is accomplished by adjusting length collimation stops sited immediately in front of the bridge in the collimation system of the Kratky camera, and by adjusting entrance slits sited immediately in front of the counter. The shape of the incident beam at the registration plane [the plane in which the slits defining the entrance width (dimension parallel to counter movement) move is shown in Figure 6. This is obtained with an infinitely narrow counter length. It is seen that $2\ell = 37.5$ mm and $2k = 7.5$ mm. The counter slit length was therefore set equal to 10 mm to satisfy equation 8. The slit may be considered infinite up to m = 15 mm which corresponds to $1/d = 0.045\ (\mathring{A})^{-1}$ in the units used to present our scattering patterns.

The desmearing is accomplished by a computer program described by Heine and Roppert[45,46]. It was acquired courtesy of Prof. W. Krigbaum at Duke University and adapted for use at R. T. I. The derivatives required (See equation 6) are obtained by use of a spline function as described below.

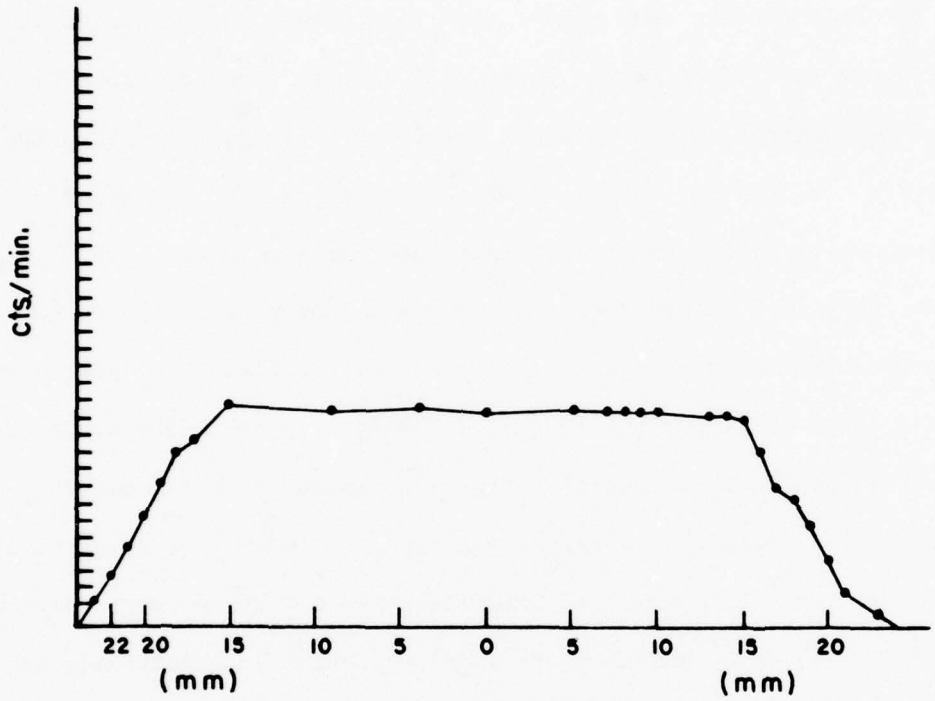

Figure 6. Actual Kratky camera incident beam profile obtained with our experimental set up.

5.1.1.4 Spline Function Approximation of Scattering Curve for Numerical Differentiation

The computer program for the desmearing process requires the derivative of the observed intensity distribution $d\tilde{I}(m)/dm = \tilde{I}'$. Graphical differentiation can be subjected to considerable errors especially in the case of steeply descending functions. For this reason, the experimental intensity data are interpolated by a collocation spline function which supplies the required derivative of the intensity distribution.

The experimental scattering intensities are plotted vs. reciprocal Bragg distances and a smooth curve is drawn by visual inspection. Points (knots) are then selected on the curve which define the interpolating spline function. The spline function as well as its first derivative are then calculated.

Further improvement of the evaluation method was obtained by a change to a natural spline for interpolation. The first spline approximation[47] required the slopes at the boundaries of the interpolation interval to be known since they are input parameters. Especially the initial slope at small scattering angle is difficult to estimate, and, consequently, errors might be introduced in the initial part of the intensity distribution. The boundary conditions for a natural spline are given by the second derivatives of the spline being zero at the boundaries, i.e., the spline starts and ends without curvature. The first derivatives at the boundaries follow from the general continuity conditions[48].

The first derivatives y_i' at the knots x_i, y_i of a natural spline

are defined by the equation system where h_i denotes $x_{i+1} - x_i$. The

$$\begin{bmatrix} \frac{2}{h_1} & \frac{1}{h_1} & & & \\ \frac{1}{h_1} & 2\left(\frac{1}{h_1}+\frac{1}{h_2}\right) & \frac{1}{h_2} & & \\ & \frac{1}{h_{i-1}} & 2\left(\frac{1}{h_{i-1}}+\frac{1}{h_i}\right) & \frac{1}{h_i} & \\ \cdots & \cdots & \cdots & \cdots & \cdots \\ & & & \frac{1}{h_{n-1}} & \frac{2}{h_{n-1}} \end{bmatrix} \begin{matrix} y'_1 \\ y'_2 \\ y'_i \\ \cdots \\ y'_n \end{matrix} = \begin{bmatrix} \frac{3}{h_1^2}(y_2 - y_1) \\ \cdots \\ 3\left[\frac{y_{i+1} - y_i}{h_i^2} + \frac{y_i - y_{i-1}}{h_{i-1}^2}\right] \\ \cdots \\ \frac{3}{h_{n-1}^2}(y_n - y_{n-1}) \end{bmatrix}$$

parameters for the cubic of the interpolation interval h_i are then derived from the equation system

$$\begin{bmatrix} 1 & x_i & x_i^2 & x_i^3 \\ 1 & x_{i+1} & x_{i+1}^2 & x_{i+1}^3 \\ 0 & 1 & 2\,x_i & 3\,x_i^2 \\ 0 & 1 & 2\,x_{i+1} & 3\,x_{i+1}^2 \end{bmatrix} \begin{matrix} a \\ b \\ c \\ d \end{matrix} = \begin{bmatrix} y_i \\ y_{i+1} \\ y'_i \\ y'_{i+1} \end{bmatrix}$$

The ordinate for the interpolated point $x_i < x < x_{i+1}$ is then given by

$$y = a + bx + cx^2 + dx^3 \qquad (10)$$

The first derivative of the intensity distribution at x is given by

$$y' = b + 2\,cx + 3\,dx^2 \qquad (11)$$

Although spline approximations are extremely well suited to representing functions which cannot be expressed in closed form and for obtaining their first derivatives, care has to be taken in the selection of the knots. Inside an interpolation interval the first derivative is given by eq. (11). If the intervals are taken too large, long segments of the derivative will follow a second order parabola, thus introducing an artifact in subsequent data manipulation. If the intervals are taken too closely spaced, reading errors become significant which show as weak undulation of the approximating spline around the actual curve. This undulation can be so weak that it remains unobservable on the spline but it becomes very pronounced in its first derivative. In order to avoid such possible pitfalls, the angular dependence of the calculated first derivatives is always checked graphically for smoothness.

5.1.2 Information Attainable From SAXS

Small angle x-ray scattering (SAXS) of solid materials is often used for semi-crystalline samples to detect repeat distances between regularly spaced lamella. This is manifested by a peak in the graph of scattered x-ray intensity versus scattering angle. For cured epoxy samples no regularly spaced alterations of electron density with repeat distances in the range 30-1000 Å are anticipated and a broad SAXS peak has been observed in only one instance (See Section 5.2.5.2).

However, SAXS is additionally capable of providing information concerning the mean density fluctuation within a sample. If we assume that such density fluctuations find their origin in two phases, each of uniform electron density caused by different degrees of crosslinking, the method can be interpreted in terms of the density difference between the two phases assuming each phase makes up 50% of the sample. In addition, the relative size of such uniform phases may be obtained as well as information relating to the actual electron density fluctuations within each phase, i.e., to what extent the assumption that each phase is of uniform electron density is actually valid. The conventional methods of extracting this data from the SAXS intensity distribution are described below.

5.1.3 Angular Nomenclature:

The angle between the incident and scattered beam is designated as 2θ. In the following discussion of the interpretation of x-ray scattering, material is drawn from a variety of sources. Unfortunately, three principal angular functions are used for consistency with the original

literature.[97] These are, for small angles

$$S = \frac{2\Theta}{\gamma}$$

$$h = \frac{4\pi\Theta}{\gamma} \qquad (12)$$

$$m = 2a\theta = a\lambda S$$

where m is the linear distance between the scattered and incident rays in the plane of registration of the Kratky camera, a is the distance between sample and the plane of registration (normally 205 mm) and λ is the wavelength of the incident x-rays (1.542 Å).

5.1.4 Guinier plot:

Guinier's treatment of SAXS scattered intensity yields a dimension for particles of electron density, differing from the mean electron density of the sample, for the case where inter-particle intereference is negligible. It is routinely used for determining the size of polymer molecules in dilute solution. In the following we explain the basis of this treatment for a system of homodisperse particles in dilute solution and then examine the effect of polydispersity and interparticle scattering, which must be considered for epoxy samples.

As x-rays impinge on a particle the electrons in that particle are forced into oscillation by the electromagnetic field of the x-rays. The electrons in turn become a source of radiation, and in this way, the electrons are said to scatter the impinging radiation. When the angle between the incident and scattered radiation is 0°, all the scattered radiation interferes constructively. But for all other angles some degree of distructive interference is inevitable, as the path length traversed by incident + scattered beam from one electron in the particle will, in general, be different from that scattered by another electron

in the same particle. Thus, the atomic scattering factor, f, the scattering by an isolated atom is proportional to the atomic number at zero scattering angle, but decreases with angle as shown in Figure 7. It is intuitively obvious that as the scattering particle increases in size, the peak at 0° will become sharper, and the shape of the curve will become steeper. Debye[50] showed that for an isolated particle for which the scattering is averaged over all possible orientations with the respect to the incident x-ray beam, the intensity of scattering may be expressed:

$$I(h) = \overline{F^2(h)} = \sum_{j=1}^{m} \sum_{k=1}^{m} f_k f_k \frac{\sin(h\, r_{jk})}{h\, r_{jk}} \qquad (13)$$

Here $h = \frac{4\,\pi \sin\theta}{\gamma}$ where $2\,\theta$ is the scattering angle (the angle between incident and scattered x-rays), λ is the wavelength of the incident radiation, f_j is the atomic scattering factor of the jth atom and r_jk is the distance in the particle between the jth and kth atom. Guinier[51] recast equation (13) as

$$\overline{F^2(h)} = \left(\sum_{j=1}^{m} f_j\right)^2 - \left(\frac{h^2}{6}\right) \sum_{j=1}^{m} \sum_{\substack{k=1 \\ j \neq k}}^{m} f_j\, f_k\, r_{jk}^{\,2} + \ldots \qquad (14)$$

by expressing $\sin\chi/\chi$ as the power series $1-\chi^2/6 + \ldots$ and retaining only the first two terms. By defining the electronic center of gravity, 0, by $\sum_j f_j \vec{r}_{oj} = 0$ and expressing equation (2) in terms of $\vec{r}_{oj}$, he showed that

$$\overline{F^2(h)} = \left(\sum_j f_j\right)^2 \left[1 - \frac{h^2 \sum f_j\, r_{oj}^{\,2}}{3 \sum f_j} + \ldots\right] \qquad (15)$$

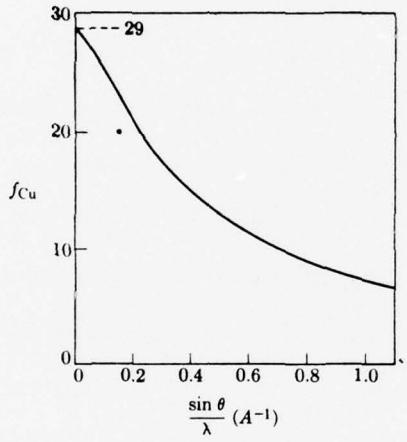

Figure 7. The atomic scattering factor of copper.

Since the term $\frac{\Sigma f_j r_{oj}^2}{\Sigma_j} = R^2$, R being the electronic radius of gyration, and the term in brackets is the power series expansion of an exponential function, the Guinier approximation is given as:

$$I(h) = \overline{F^2(h)} = (\Sigma_j f_j)^2 e^{-\frac{h^2R^2}{3}} \qquad (16)$$

Thus one can obtain the radius of gyration, R, of a particle from the initial slope of the Guinier plot, ln I(h) vs h^2.

One can obtain further information concerning the shape of the particle from Guinier plots in which ln h I(h) or ln h^2I(h) are plotted versus h^2. Such plots would be linear (at scattering angles higher than those used for the initial slope) for rods or plate-like particles respectively. But as a spherical shape would appear to be the best assumption for the type of particle to be expected in a cured epoxy resin and polydispersity and interparticle interferences would preclude such detailed analysis in any case, no effort has been made to analyze the data in this way.

The radius of gyration must be obtained from data near the origin of the ln I vs h^2 plot. It is necessary to define the point at which the ln I versus h^2 plot will deviate significantly from that predicted by Guinier's law. For spherical particles[52] Guinier's approximation is an accurate presentation of the scattering curve up to $h \cdot R = 1.3$, after which the actual curve falls below that predicted by Guinier's approximation. For rod like particles Guinier's approximation is a good approximation up to $hR = 0.7$, after which the actual curve rises above that predicted by Guinier's approximation. Particles which are in the shape of an ellpise would be intermediate between these two and if the

major and minor axes differ only slightly, the Guinier approximation would be good to scattering angles somewhat higher than hR = 1.3.

5.1.4.1 Effect of polydispersity:

The radius of gyration, as obtained from the Guinier plot, tends to favor the largest particles heavily.[53] When expressed in terms of m (Ro) dRo, which gives the total mass of particles whose radius of gyration is contained between Ro and Ro + dRo, the mean observed radius of gyration, R_{om} is given as:

$$R_{om}^2 = \frac{\int m\,(R_o)\,R_o^5\,d\,R_o}{\int m\,(R_o)\,R_o^3\,d\,R_o} \qquad (17)$$

5.1.4.2 Effect of Interparticle Interference:

For particles of uniform size, interparticle interference causes the initial part of the I(h) versus (h) curve to decrease and therefore decreases the slope of curve close to the incident beam. This effect is the more pronounced, the higher the concentration of particles. For a heterogeneous mixture of particles the deviations from the scattering phenomena calculated for isolated particles is less marked. In fact, Guinier and Fournet state:[54] "in a mixture of non-identical particles of arbitrary forms and with random distribution (no long-range order) it is improbable that the packing of particles will lead to large changes in the scattering curves and that thus the laws for widely separated particles can furnish the orders of magnitude of the scattering phenomena".

5.1.5 The Invariant and Scattering Power of the Sample:

The mean square fluctuation of electron density $\overline{(\rho-\bar{\rho})^2}$ is the only quantity that can be obtained from the small angle x-ray scattering data, without assumptions concerning the nature of the inhomogeneities.

The quantity, $\overline{(\rho-\bar{\rho})^2}$ is called the scattering power of the sample and may be obtained from absolute intensity data by means of the relations:[49,55]

$$\overline{(\rho-\bar{\rho})^2} = P_o\left(\frac{4\pi}{i_e N^2}\right)\frac{1}{da\lambda^3}\int_o^\infty m^2 I(m)\,dm. \qquad (18)$$

Absolute intensity data means that the ratio of scattered intensity to the intensity of the incident x-ray beam is known. This ratio is routinely obtained for our samples by measuring the intensity of scattering of a standard Lupolen sample at 150 Å which has been calibrated[56] so that the ratio of the measured scattering intensity to the intensity of the incident beam is known. In equation 18

m = distance between the incident and scattered rays in the plane of registration in centimeters.

a = specimen to registration plane distance, normally 20.5 cm for the Kratky camera.

d = specimen thickness in centimeters

λ = wavelength of the x-rays, for Cu K_α, 1.5418×10^{-8} cm.

$i_e = 7.9 \times 10^{-26}$, the Thomson scattering constant of a free electron

N = Avogadro's number

P_o = Intensity of the incident x-ray beam.

Equation 18 assumes that the data has been obtained using pinhole collimation or has been desmeared. Slit smeared data may be used without

desmearing using the relation:

$$\overline{(\rho-\bar{\rho})^2} = P_o \frac{2\pi}{i_e N^2} \frac{1}{da\lambda^3} \int m \tilde{I}(m)\, dm \qquad (19)$$

This differs from equation 18 in that m, rather than m^2, is included in the integral and the integral is multipled by a factor half of that used in equation 18. The integrals in equation 18 and 19, have been called the invariant by Porod[57] and are designated by the symbols:

$$Q_m = \int_o^\infty m^2 I(m)\, dm$$
$$\tilde{Q}_m = \int_o^\infty m \tilde{I}(m)\, dm \qquad (20)$$

These quantities will depend only on the scattering power of the sample and will be unaffected by the size of domains of uniform electron density as long as the size is large enough (greater than 100 Å) to yield scattering in the small angle region.

If one assumes that a specimen may be approximated by a two-phase model, each of uniform electron density, then the scattering power is given by

$$\overline{(\rho-\bar{\rho})^2} = (\rho_1-\rho_2)^2 W_1 W_2 \qquad (21)$$

where ρ_1 and ρ_2 are the electron densities of the two phases, and W_1 and W_2, the respective volume fractions.

5.1.6 Determination of the Invariant, the Specific Surface, and Uniformity of Electron Density over Small Distance.

As seen by equations 20 determination of the invariant requires knowledge of the function $m^2 I(m)$ or $m \tilde{I}(m)$ at a scattering angle close to zero, where data cannot be obtained because of the presence of the

incident x-ray beam and at large angles where the scattered intensity is too weak to measure accurately. Errors in approximations made for the scattered intensity close to the incident beam will not affect the invariant greatly because of weighting by m or m^2 but by the same token, errors at large angles will be very important.

If data is obtained to small enough angles, it is found that the curve of Im^2 or $\tilde{\gamma}m$ begins to decrease with decreasing angle and an extrapolation to m = 0 is possible. This allows estimation of the quantity $\tilde{\gamma}m$ or Im^2 at scattering angles smaller than those experimentally attainable. The scattering intensity at very high angles can be obtained by using the theoretical finding that $h^4I=k$ in the high angle region as discussed in the next section.

5.1.7 The Correlation Function, Specific Volume, and Transversal Distance.

The correlation function $\gamma(r)$ has been defined as follows by Debye et al[58] as well as by Porod,[57] who refers to it as the characteristic:

$$\gamma(r) = \frac{\overline{(\Delta\rho)_1 \cdot (\Delta\rho)_2}}{\overline{(\Delta\rho)^2}} \qquad (22)$$

Here $(\Delta\rho)_1$ and $(\Delta\rho)_2$ are the local fluctuations of electron density at points 1 and 2, separated by the distance, r, from the average electron density, $\bar{\rho}$, and $\overline{(\Delta\rho)^2}$ is the average value of the square of such fluctuations. This function will vary from 0 when r is very large to 1 when r = 0. It is related to the intensity of scattered radiation by Fourier transformation:[57]

$$I(h) = 4\pi \int_o^\infty \gamma(r)\, r^2\, \frac{\sin hr}{hr}\, dr \qquad (23)$$

$$\gamma(r) = \frac{1}{2\pi^2} \int_o^\infty h^2\, I(h)\, \frac{\sin hr}{hr}\, dh \qquad (24)$$

The relationship existing between I(h) and $\gamma(r)$ is therefore analogous to the one which exists between the Patterson function and the distribution of (hkl) intensities of conventional crystal structure analysis.

For an isolated particle, $\gamma_o(r)$, the correlation function of the isolated particle is given by the expression:

$$\gamma_o(r) = \frac{\bar{V}(r)}{V} \qquad (25)$$

Here $\bar{V}(r)$ is the average volume common to the particle and an identical particle (its ghost) displaced by the vector r for all directions of the vector. The volume common to a particle and its ghost is shown for one direction of the vector, in Figure 8.

If we begin at any arbitrary point within the particle, and lay down a ruler of length r in any direction, then $\gamma_o(r)$ also expressses the probability that the other end of the ruler will also fall within the particle. The function $\gamma_o(r)$ is plotted as a function of r for a sphere of radius, R, in Figure 9.

For any two phase system, it can be shown that the slope of the characteristic at r = o is given:

$$\left(\frac{d\gamma}{dr}\right)_{r=o} = \frac{1}{4c(1-c)}\, \frac{S}{V} \qquad (26)$$

where V is the volume of the phase of volume fraction, c, and S is the surface area between the two phases. From the definition of $\gamma(r)$, equation 22, it is clear that $\gamma(0) = 1$. However, the greater the surface

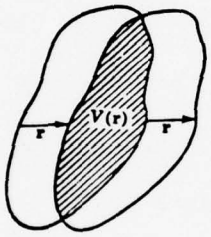

Figure 8. A representation of the function of $\bar{V}(r)$.

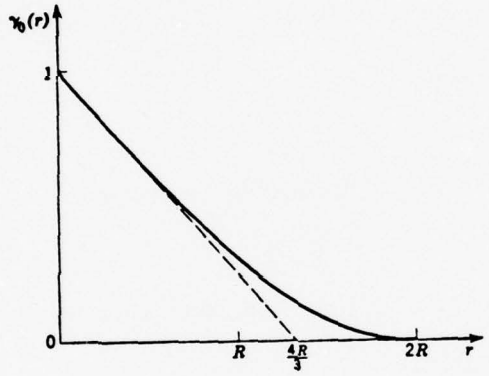

Figure 9. The function $\gamma_o(r)$ for the sphere of radius R.

to volume ratio (the specific surface, S/V), the greater the probability that "rulers" of r close to zero will lie with one end in one phase and the other in the other phase. Each "ruler" with ends in different phases contributes zero to $\gamma(r)$, hence contributing to the decrease of $\gamma(r)$ with r close to $4 = 0$.

The specific surface can be obtained from the part of the small angle scattering curve at high angles. This follows from the fact that since $hI(h)$ and $r\gamma(r)$ are related by a Fourier transform (See equations 23 and 24), the high angle part of the curve of I(h) corresponds to the part of the curve of $\gamma(r)$ at small values of r. It can be shown[57,58] that as a consequence of this

$$h^4 I(h) = k \tag{27}$$

for pinhole collimation or for a desmeared curve and

$$h^3 \tilde{I}(h) = k_1 \tag{28}$$

for a smeared intensity distribution. The specific surface can then be obtained from the relationship

$$S/V = \frac{2\pi^2}{\lambda a} c(1-c)\frac{k}{Q} \tag{29}$$

or

$$S/V = \frac{8\pi}{\lambda a} c(1-c)\frac{k_1}{\tilde{Q}} \tag{30}$$

where a is the sample to registration plane distance, c is the volume fraction of one phase and Q (or $\tilde{Q}$) is the invariant as defined by equations 20.

For an irregular two-phase system of phases 1 and 2 the specific surface may be related to <u>transversal lengths</u> as illustrated in figure 10. The average intersection of arrows (in all directions) with each

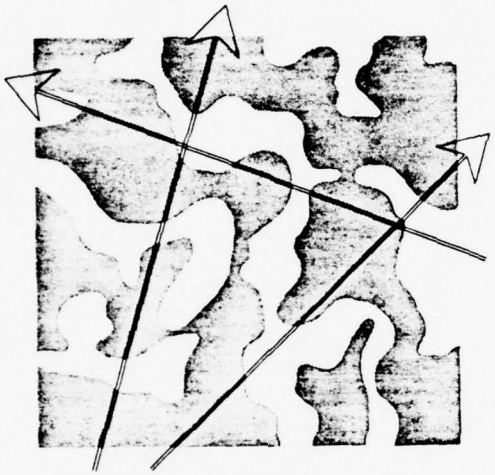

Figure 10: Physical concept of the transversal length.

phase are given by:

$$\bar{\ell}_1 = \frac{4\ W_1}{S/V} \tag{31}$$

$$\bar{\ell}_2 = \frac{4\ W_2}{S/V} \tag{32}$$

where W is the volume fraction of each phase. Debye, Anderson and Brumberger[58] have shown that for a random distribution of two phases

$$\gamma(r) = \exp \frac{-r}{\bar{\ell}_c} \tag{33}$$

$$\text{for which } \frac{1}{\bar{\ell}_c} = \frac{1}{\bar{\ell}_1} + \frac{1}{\bar{\ell}_2} \tag{34}$$

$$\text{and } S/V = \frac{4\ W_1\ W_2}{\bar{\ell}_c} \tag{35}$$

The quantity, $\bar{\ell}_c$, is termed the correlation distance. According to Debye, Anderson and Brumberger, the intensity of scattering for such a random two-phase sytem is given as:

$$I(h) = \frac{A}{(1 + h^2\ \bar{\ell}_c^{\,2})^2} \tag{36}$$

A plot of $(I(h)^{-1/2}$ versus h^2 should yield a straight line whose slope-intercept ratio would yield $\bar{\ell}_c$

$$\bar{\ell}_c = \frac{\lambda}{2\ \pi} \left(\frac{\text{slope}}{\text{intercept}} \right)^{1/2} \tag{37}$$

It would appear that the product $W_1 \cdot W_2$ can be obtained from determination of $\bar{\ell}_c$ from equation 37 and of S/V from equation 29 or 30. This would then yield the transversal lengths, ℓ_1 and $\bar{\ell}_2$.

In practice, the high angle region of the small angle scattering curve will usually be given by an expression of the type:

$$\gamma_I(h) = \frac{k_1}{h^3} + k_2 \tag{38}$$

rather than by equation 28. The additional term k_2 is caused by fluctuations of electron density at small distances[59] (deviations from the assumption that each phase is of uniform electron density). Such a term is particularly noticable for slit smeared data because the smearing is caused by the addition of higher angle intensity data to a given I(h) (See equation 4).

Additionally, the assumption is made that the transition from one phase to the other is sharp in the derivation of eqs. 27 and 28. A zone of gradual transition would tend to decrease the deserved k or k_1. Methods for estimating the size of the zone of gradual transition between phases, as well as accurate determination of k_2 (eq. 38) and S/V (eqs. 29 & 30) are discussed by Ruland.[60]

5.1.8 Swelling Sample as a Means of Modifying SAXS.

As SAXS is sensitive to electron density variation within a sample, the changes that occur in the SAXS of a sample after swelling can yield useful information. For example, where SAXS is caused by voids accessible to a solvent, the SAXS would be largely wiped out by when solvent fills the voids. Where a lightly cross-lined region differs little in density from a tightly cross-linked zone, but is much more accessible to solvent, permeation of heavy atom containing solvent might increase SAXS due to an increase in electron density contrast. The same effect might be obtained if it were possible to react a heavy atom containing curing agent with a tetrafunctional epoxy molecule only after the first two functions are satisfied, i.e., only when epoxy molecule is involved in cross-linking.

5.1.9 Application of Heavy Atom Tagging to Spatial Distribution of Cross-links

The method of elucidating the spatial distribution of cross-links by heavy atom tagging requires that two conditions be fulfilled. Firstly, the heavy atoms must be identified with cross-links and not be present in parts of the network in which not all functionalities of the epoxy or hardener molecules are satisfied leading to non-cross-linked chains. Secondly, interference from scattering by non-heavy atom components must be accounted for. This is particularly important for epoxy networks for which cross-links are so closely spaced that the distances between them would be expected to fall in the range of 5-15 Å.

This is seen on consideration of the equation for the scattering from an isotopic sample

$$I(s) = \sum_n \sum_m f_m f_n \frac{\sin(sr_{mn})}{sr_{mn}} \qquad (39)$$

where f_m and f_m are the atomic scattering factors of the mth and nth atoms and r_{mn} is their separation. The heavy atom method works because the atomic scattering factor is much larger for the heavy atoms than for lighter atoms such as carbon, oxygen and nitrogen. If we use the subscript L for the light atoms and H for heavy atoms, the vector r_{HH} is weighted to a considerably greater extent in equation 39 than r_{LL} or r_{LH}. However, in the range of 5-15 Å this advantage is overcome to some extent by the fact that the number of light atoms is greater than that of the heavy atoms and they tend to distribute themselves in such a fashion that certain values of r_{LL} occur with great frequency. This leads to peaks in the WAXS pattern for epoxy resins (containing no heavy

atoms) with Bragg values corresponding to approximately the most favored value of r_{LL}. It then becomes necessary to devise a second sample which will have the same r_{LL} and r_{LH} distribution as the sample of interest so that only the r_{HH} distribution differs. The desired information concerning the distribution of r_{HH} can then be obtained by subtracting the WAXS pattern of the second sample from that of the first. Such schemes have been applied by Brady et al[61,62] and Li, Post and Morawetz[63] to heavy atom tagged polymeric molecules in solution. Brady subtracted the x-ray scattering pattern of heavy atom labelled monomer in solution from that of heavy atom labelled polymer in solution. Li, Post and Morawetz[61] used the scattering from solutions of oligomers tagged at both ends with iodine. The L-H interactions in the molecule and with the solvent were corrected for by subtracting the x-ray scattering from solutions of the corresponding oligomer tagged at only one end, yielding the end to end distance in the diiodo-oligomer.

5.2 Results of X-Ray Scattering from Cured Epoxy Samples

5.2.1 Introduction

The strategy in obtaining small angle x-ray scattering (SAXS) data has been to select series of samples in which trends might be expected to be followed from sample to sample, concerning the sizes of highly cross-linked clusters. SAXS data was then interpreted according to the methods described in sections 5-1 of this report with results compared to those expected. This provided a degree of confidence in the x-ray results as compared to a situation in which such results would have to be blindly accepted.

The samples included in this report are taken from those given in Tables I and II. They include D-1, D-2, D-3, and D-4 which were all

cured at 120°C with varying amounts of unreactive diluents. Additionally, samples Q-1, Q-7, and Q-8 were cured at temperatures of 80°C, 130°C and 180°C respectively. For these samples an increase in nodule size with increased curing temperature is expected on the basis of the nucleation theory of Lüttgert and Bonart.[8] Finally samples Q-3, and Q-4 were examined. Sample Q-3 was cured at 80°C, but then annealed at 120°C and finally at 140°C. Sample Q-4 was cured at 80°C with only 0.6 mol anhydride per mol epoxy groups. All other Q samples examined had been cured with 0.9 mol anhydride per mol epoxy groups.

The interpretation of the small-angle xray scattering data can be divided into three parts: 1) Calculation of the scattering power of the sample from the total SAXS data (See eq. 18), 2) Determination of the size of clusters of high (or low) density relative to the mean sample density from the shape of the SAXS curve close to the main beam, and 3) determination of the correlation distance, $\bar{\ell}c$, and specific surface, S/V, from the intensity of scattering in the tail end of the SAXS curve relative to the invariant. In attempting to carry out the first two evaluations, it became clear that the resolution of the Kratky camera used to obtain the SAXS data was too low. As a result we are presently aligning a newer Kratky camera with a smaller entrance slit to achieve higher resolution. However, the data at high angles did yield results in line with expectations. The evaluations are described in detail below.

5.2.2 Experimental

SAXS data was obtained using a Kratky camera with a 40 μm entrance slit and a 100 μm or 200 μm counter slit. A Siemens Kristalloflex 4 x-ray generator using a Kratky tube with copper target is used to supply

x-ray flux. The counts are detected using an LND Xenon filled proportional counter and Siemens preamplifier and Siemens 19" counting panel. Automatic step scanning is carried out by using a Humphrey step Scan 721 with data recorded automatically on a printer. Monochromatization is by means of a nickel filter and pulse height discrimination. The x-ray equipment is housed in a small individually thermostated room to minimize temperature fluctuations.

The intensity data from the sample is corrected for absorbtion of Cu K_α x-ray in the sample and for long term fluctuations in the x-ray flux from the generator. Such fluctuations are monitored by measuring the scattering from a Lupolen standard at 2-4 hour intervals. This also allows scattering data to be placed on an absolute scale as the standard is calibrated with respect to the flux of the incident beam.[56] When data is taken overnight, scans are repeated at 2-3 hour intervals so that long term fluctuations are averaged over all the data and can be recognized by scanning the counts for each scan. Background data is taken in the same way as sample data and corrected for the intensity of the incident beam. Background data is then subtracted from the sample data to obtain the xray scattering from the sample. The data is desmeared as described in section 5.1.1 of this report.

5.2.3 Scattering Power

The evaluation of scattering power involves calculation of the invariant as shown by eqs. 18, 19 and 20. Although it is impossible to obtain data at infinitely small angles as required for the integrals in the cited equations, $\tilde{\gamma}\cdot m$ or $I\cdot m^2$ will decrease with decreasing angle, if data is obtained to sufficiently small angles, permitting extrapolation to zero angle. Such an extrapolation was not possible for the data we

obtained as $\tilde{\gamma} \cdot m$ increased with decreasing angles at the smallest angles for which scattered intensity was recorded. This indicated that scattering intensities at higher resolution should be obtained.

5.2.4 Evaluation of Scattering Intensity at Very Small Angles

Two methods are available for analyzing the shape of the scattered intensity plotted against scattering angle to obtain the extent of regions of high or low density within the sample. These are the Guinier plot and the method of obtaining the correlation distance, $\bar{\ell}_c$, described by Debye et al[58] (See eqs. 33-37). Evaluation by both methods was attempted. The trends obtained with the Guinier plot were in line with those expected. However, both methods of evaluation indicated that better data was needed at extremely low angles.

5.2.4.1 Guinier Plots

The size of an isolated particle can be derived from the shape of the SAXS curve close to the main beam from the slope of a ln(h) vs h^2 plot (Guinier plot). In the absence of interparticle interference effects, the scattering from a collection of particles will equal the sum of the scattering curves from each individual particle. For cross-linked epoxy, clusters of high density would be expected to be of arbitrary form and with a random distribution, thus minimizing interference effects. Additionally, the physical basis for the interpretation of SAXS data by the Guinier plot is easily understood and thus serves as a logical first approximation in presenting SAXS results.

The radii of gyration derived from Guinier plots are presented in Table III. In some cases two straight line segments were observed on the Guinier plot as shown in Figure 11. In these cases two radii of gyration are reported for the same sample. It may be seen that the introduction

TABLE III. CLUSTER DIMENSIONS FROM SAXS.

Sample Designation	Anhydride Kind	Anhydride R_H	Diluent Kind	Diluent ml/g	Curing Temperature (s) (°C)	Radius of Gyration (Å)	Ruland plot Intercept $\frac{(cts/min)\ (mm)^4}{cm\ of\ sample}$	Ruland plot Slope $\frac{(cts/min)(mm)^2}{cm\ of\ sample}$	k_2* $\frac{(cts/min)}{cm\ of\ sample}$
D-1	THPA	0.9	DMP	0.88	120	489			3300
D-2	THPA	0.9	DMP	0.44	120	515			3400
D-3	THPA	0.9	DMP	0.22	120	540			1940
D-4	THPA	0.9	-	-	120	532, 380			1140
Q-1	NMA	0.9	-	-	80	498, 270	251	122	1715
Q-7	NMA	0.9	-	-	130	410, 260	494	366	2050
Q-8	NMA	0.9	-	-	180	400, 190	612	504	1960
Q-3	NMA	0.9	-	-	80, 120, 140	650	23	0	1750
Q-4	NMA	0.6	-	-	80	540, 206	205	612	1570

* See Equation 38.

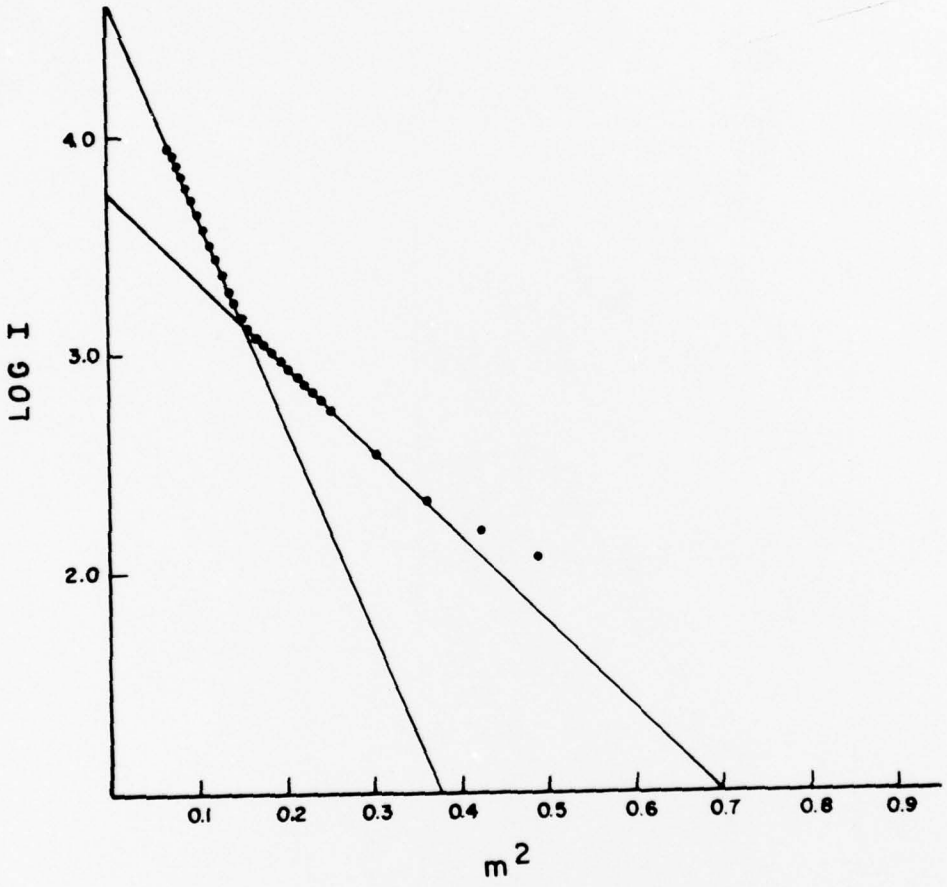

Figure 11. Guinier plot (ln I vs m^2) for sample Q-7.

of nonreactive diluent appears to decrease the size of clusters. Additionally, the expected trend of smaller cluster size with increasing curing temperature is observed for samples Q-1, Q-7 and Q-8. As stated in section 5.1.4 of this report, Guinier's law is an accurate representation of the scattering from a sphere up to $h \cdot R = 1.3$. When this criterion is applied to the radii of gyration given in Table III, it is found that data should have been obtained at considerably lower angles for such radii of gyration to be meaningful. In addition, scattering from the sample represents only 5% of the scattering intensity we have collected at the smallest angles (the rest is background scattering). For these reasons we have aligned a newer Kratky camera (on which the bridge has been redesigned) using a smaller entrance slit (19 μm). Our first results show that sample scattering represents 50% of the counts at a resolution of 3000 Å as compared to 5% at 1000 Å with the older camera. There also appear to be significant errors in the data from which the radii of gyration in Table III were obtained.

The trends in Table III are therefore encouraging and indicate that SAXS is sensitive to changes in epoxy curing conditions. However, better data is needed before the numerical values can be taken seriously. The differences in the numerical values would be expected to be somewhat larger when obtained on the newer camera.

5.2.4.2 Correlation Distance From Very Low Angle Data

The intensity data for the samples in Table III was plotted as suggested by Debye et al[58] to obtain a correlation distance, $\bar{\ell}c$, in a random two-phase system (see eq. 37). The data extrapolated to a negative intercept. This has no physical meaning and may indicate that the data at very small angles is too high, as found in initial comparisons

of SAXS from the same sample measured on both the old and new Kratky camera.

5.2.5 Evaluation of Tail of SAXS Curve

5.2.5.1 Introduction:

The specific surface or correlation distance may be obtained from the intensity of scattering at the tail of the SAXS curve. This method of evaluation has two advantages. First, the interpretation of the data is unambiguous and equally valid for dilute and condensed systems. Secondly, the data is easily obtained as background scattering is always relatively low at the tail of the SAXS curve. However, evaluation of the SAXS intensity at the tail requires knowledge of the invariant (eq. 20) which implies that SAXS data must be available to sufficiently small angles that an extrapolation of $I \cdot m^2$ or $\tilde{\gamma} \cdot m$ to zero scattering angle can be made.

5.2.5.2 Background Caused by Electron Density Variations Within Phases

SAXS data is commonly found to contain a component which is independent of scattering angle as given by the constant, k_2, in equation (38). This is commonly ascribed to fluctuations of electron density within the phases of extent large enough to give rise to SAXS. This component must be subtracted from the SAXS spectrum before further evaluation. This is automatically accomplished in the desmearing operation.

The constant, k_2, is given in the units, counts/min per cm. of sample (to correct for the effects of sample thickness) in Table III. It may be seen that the introduction of non-reactive diluent raises the background due to non-uniform density in individual phases. The wide angle x-ray scattering pattern shows that the non-reactive diluent

separates into a distinct phase, at least in part. For sample D-1, two broad peaks are seen in the WAXS photograph corresponding to Bragg spacings of 5.2 and 12.5 Å. For samples D-2, D-3 and D4, these rings are visible, with the addition of another peak corresponding to a Bragg spacing of 6.6 Å. Additionally, the 12.5 Å peak has moved to a smaller angle, corresponding to 15.5 Å. Microdensitometer traces and the Bragg spacings obtained are shown in Figures 12, 13 and in Table IV respectively for samples D-1 and D-4.

A broad peak is obtained in the desmeared SAXS intensity plot for sample D-1 as shown in Figure 14. The peak corresponds to a Bragg spacing of 300 Å. No such peak was noted for any of the other samples.

The increased liquid-like disorder in the samples containing DMP may be intrinsic to the DMP phase or to increased density fluctuation within the epoxy phase caused by the DMP.

5.2.5.3 Evaluation of Specific Surface and Correlation Distance

The specific surface can be obtained from the tail of the SAXS intensity distribution by identifying the part of the curve where $h^4 I(h) = k$ or $h^3 \gamma(h) = k_1$. The specific surface can be related to a correlation distance, $\bar{\ell}c$, as shown by equations 29, 30 and 35. We have found that a variation of this approach suggested by Ruland yields reasonable results for the Q series of samples. Ruland pointed out that two distinct phases were assumed with an infinitely sharp density transition from one phase to the other. The consequence of assuming a finite width to the transition zone (rather than a sharp transition) is that $S^4 \cdot I$ will not be a constant but will decrease as a linear function of S^2 at the tail of the SAXS intensity distribution. In a plot of $S^4 \cdot I$ versus S^2, the intercept at S=0 will equal k which can be related to S/V and $\bar{\ell}_c$ by

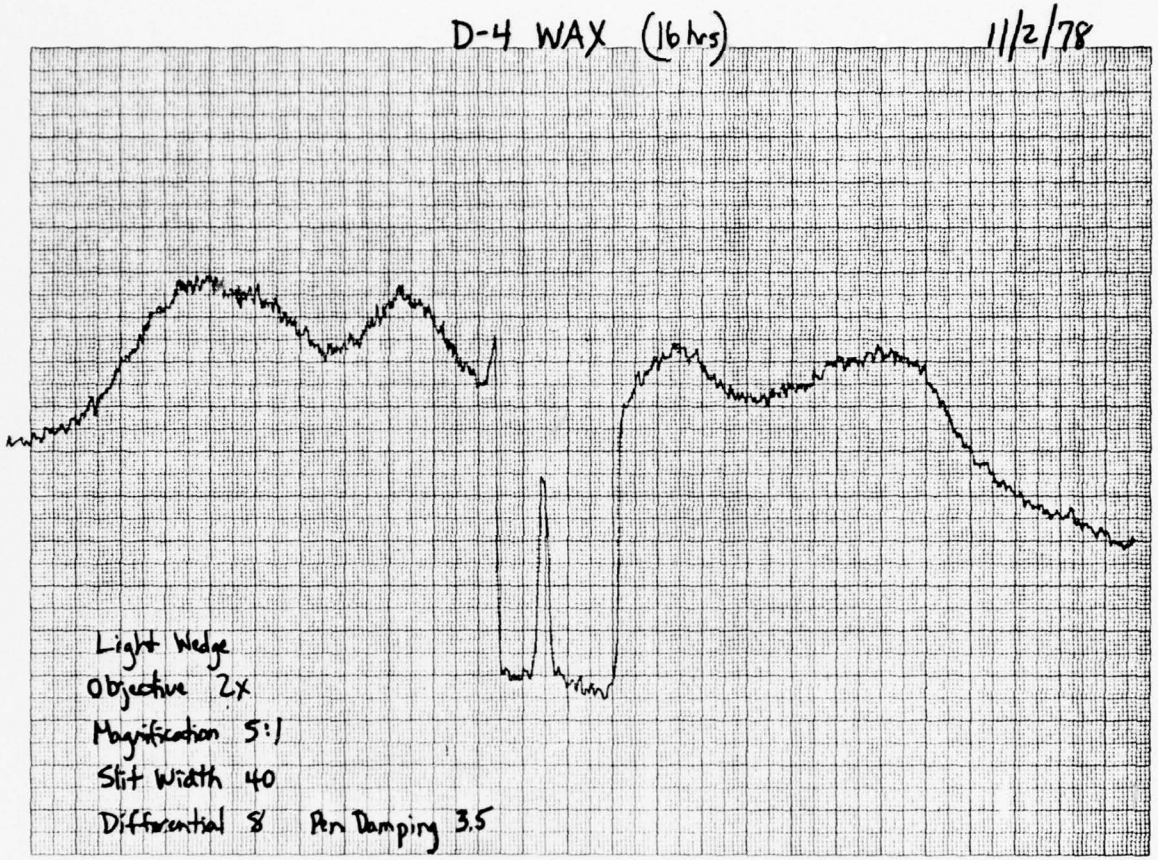

Figure 12. Microdensitometer trace of WAXS flat plate photograph obtained for sample D-4. The dip in the middle represents the beam slope shadow with a peak indicating the intersection of the main beam with film.

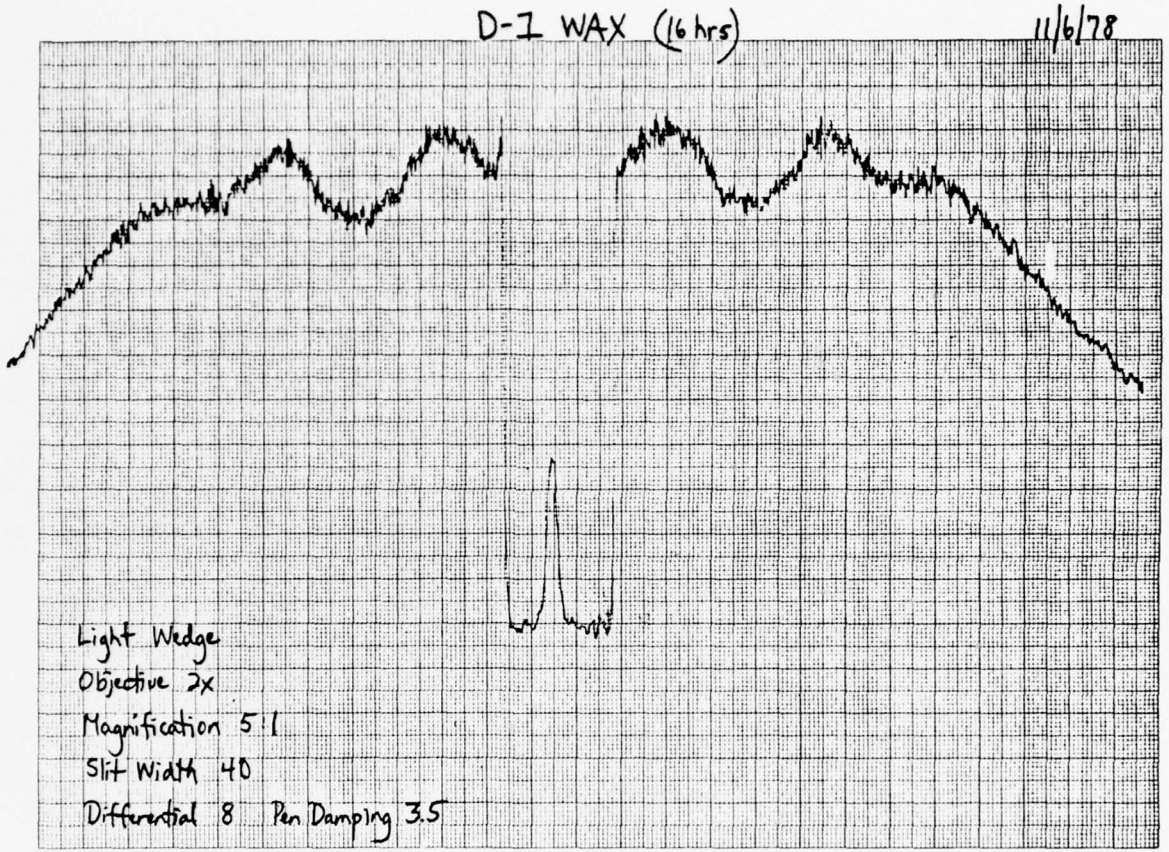

Figure 13. Microdensitometer trace of WAXS flat plate photograph obtained for sample D-1.

TABLE IV

Bragg Spacings froms WAXS Photographs

Sample Description	Bragg Spacings Å (A)
D-4	5.2 12.5
D-1	4.7 6.6 15.5

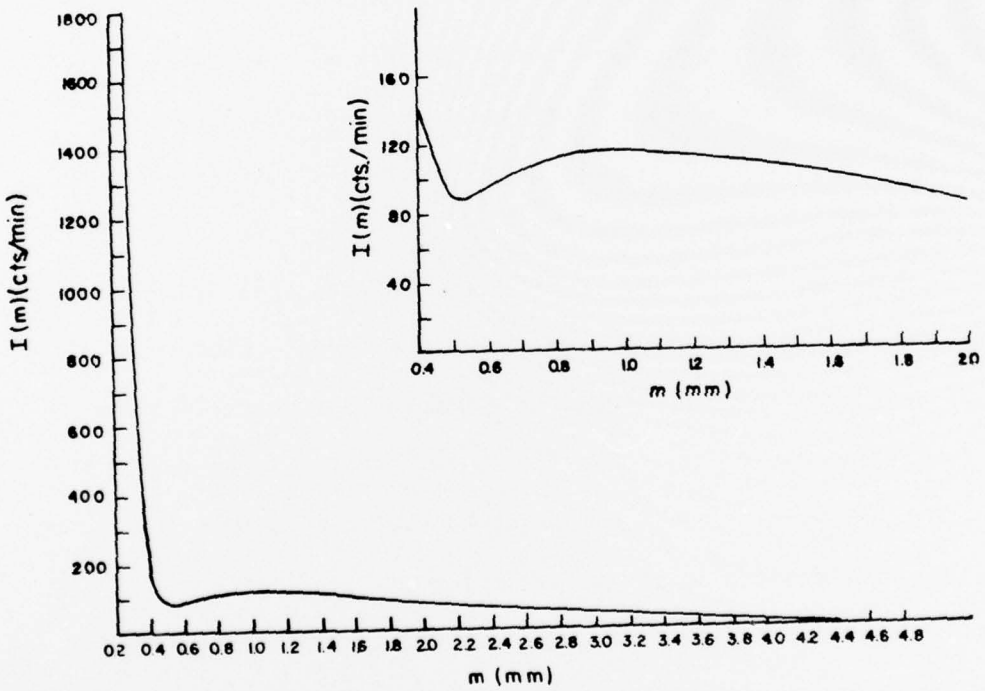

Figure 14. SAXS intensity distribution as a function of the distance (m) of detector slit from the intersection of incident beam with the plane of registration of the Kratky camera. Desmeared data for Sample D-1.

equation 29 and 35 and the slope is equal to:

$$- \frac{8 Q_S s^2 \sigma^2}{\bar{\ell}_c}$$

where Q_S is the invariant and σ^2 is a parameter related to the finite width of the transition zone. Plots of $m^4 \cdot I$ versus m^2 have been made for the samples listed in Table III. Such a plot is shown in Figure 15 and the slopes and intercepts are given in Table III. These values are not converted to specific surfaces because we have been unable to calculate the invariant from the SAXS data presently at our disposal. However, if we assume that the invariant does not vary drastically from sample to sample, the slopes and intercepts listed in Table III are consistent with larger specific surface (smaller correlation distance) for the sample cured at 180°, Q-8, with a trend to larger correlation distance as the curing temperature decreases (See data for Q-7, Q-1). The extent of the transition zone relative to the correlation distance also decreases with decreasing curing temperature. Of particular interest is the result for Q-3 which indicates that the extent of a homogeneous phase (presumably highly cross-linked) is very large for a sample cured first at 80, then at 120 and finally at 140. It may be noted that this sample also showed an unusually steep slope in the Guinier plot.

It was not possible to find a zone at comparably high angles for which $m^4 I$ varied as a function of m^2 for the D series of samples. This may be caused by the tail of the wide angle peak of 15 Å Bragg spacing contributing to the SAXS intensity distribution. For sample D2, D3, and D4 interphase interference of the type shown in Figure 14 also contributes to the SAXS intensity distribution in the part of the curve to which the above analysis is applied. Because it is not possible to separate the two effects, the analysis cannot be carried out for these samples.

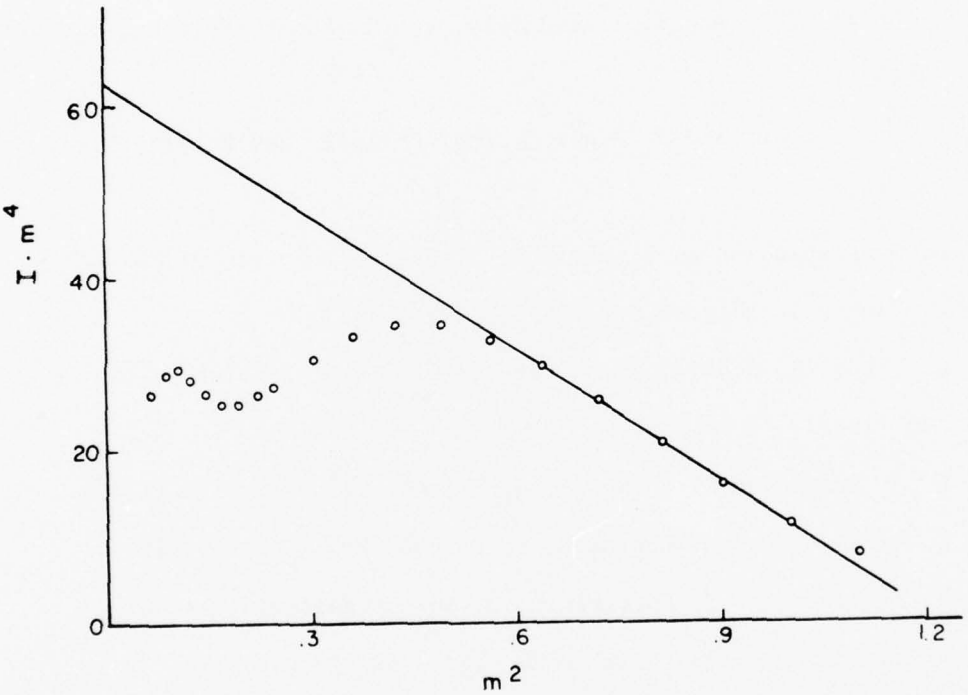

Figure 15. Plot of $I \cdot m^4$ versus m^2 for sample D-8.

References

1. W. Funke, Chimia, 22, 111 (1968).
2. W. Funke, W. Beer, and U. Seitz, Progr. Colloil. & Polymer Sci., 57, 48 (1975).
3. K. Dusek, Polymer Letters, 3, 209 (1965).
4. K. Dusek, J. Polymer Sci., C16, 1289 (1967).
5. T. G. Fox and S. Loshaek, J. Am. Chem. Soc., 75, 3544 (1953).
6. W. Fisch, W. Hofmann, and R. Schmid, Chimia, 22, 108 (1968).
7. K. Dusek, J. Plestil, F. Lednicky, and S. Lunak, Polymer, 19, 393 (1978).
8. K. E. Lüttgert and R. Bonart, Prog. Colloil. and Polymer Sci., 64, 38 (1978).
9. A. S. Kenyon and L. E. Nielson, J. Macromol Sci., A3, 275 (1969).
10. W. Funke, J. Polymer Sci., C16, 1497 (1967).
11. F. Lohse, R. Schmid, H. Batzer and W. Fisch, British Polymer J., 1, 110 (1969).
12. E. H. Erath and R. A. Spurr, J. Polymer Sci., 35, 391 (1959).
13. E. H. Erath and M. Robinson, J. Polymer Sci., C3, 65 (1963).
14. V. Ye.Basin, L. M. Korsunskii, O. Yu. Shokalskaya, and N. V. Aleksandrov, Polymer Sci. USSR, 14, 2339 (1972).
15. R. E. Cuthrell, J. Appl. Polymer Sci., 11, 949 (1967).
16. K. Selby and L. E. Miller, J. Material Sci., 10, 12 (1975).
17. J. L. Racich and J. A. Koutsky, J. Appl. Polymer Sci., 20, 2111 (1976).
18. R. Schmid, Progr. Colloiol & Polymer Sci., 64, 17 (1978).
19. R. M. Kessenikh, L. A. Korshunova, and A. V. Petrov, Polymer Sci. USSR, 14, 466 (1972).

20. H. F. Wohnsiedler, J. Polymer Sci., C3, 77 (1963).

21. L. A. Sukhareva, Yu. P. Kovrizhnykh, and P. I. Zubov, Polymer Sci. USSR, 11, 2147 (1969).

22. T. E. Lipatova, V. K. Ivashchenko, and L. I. Bezruk, Polymer Sci. USSR, 13, 1913 (1971).

23. N. N. Kiryukhin, A. M. Ogrel, A. F. Puchkov, and A. P. Khardin, Polymer Sci. USSR, 13, 2152 (1971).

24. J. L. Racich and J. A. Koutsky, ACS Coatings and Plastics Preprts., 3612, 695 (1976).

25. J. L. Kardos, N. Y. Acad. Sci., 35, 136 (1973).

26. R. J. Morgan and J. E. O'Neal, ACS Coatings and Plastics Preprts., 3G/2, 689 (1976).

27. O. Kratky, G. Porod and Z. Skala, Acta Phys. Austriaca, 13, 76 (1960).

28. A. Belkebir-Mrani, G. Beinert, J. Herz, and A. Mathis, European Polymer J., 12, 243 (1976).

29. J. E. Herz, P. Rempp, and W. Borchard, Adv. High Polymer, 26, 105 (1978).

30. H. Benoit, et al., J. Polymer Sci., Phys. Ed., 14, 2119 (1976).

31. W. Fisch and W. Hofmann, Makromol. Chem., 44/46, 8 (1961).

32. Y. Tanaka and M. Kakiuchi, J. Appl. Polymer Sci., 7, 1951 (1963).

33. R. F. Fischer, J. Polymer Sci., 44, 155 (1960).

34. K. Dusek, M. Bleha and S. Lunak, J. Polymer Sci., Chem. Ed., 15, 2393 (1977).

35. V. F. Kucherov, A. L. Shabanov, and A. S. Onishchenko, Chem. Abst., 59:7381 h.

36. R. S. Wilder and G. D. Martin, U. S. Pat. 2,550,744, Chem. Abst. 46: 2574 g.

37. G. T. M. VanderKerk, J. G. Noltes and J. G. A. Luijten, J. Appl. Chem., 1, 366 (1957).

38. G. H. Reifenberg and W. J. Considine, J. Orgmet. Chem., 9, 505 (1967).

39. W. P. Neumann, H. Niermann and R. Sommer, Am. Chem., 659, 27 (1962).

40. G. Smith, U. S. Pat. 3,332,970.

41. A. Guinier & G. Fournet, J. Phys. Rad., 8,345 (1947).

42. A. Guinier & G. Fournet, "Small Angle Scattering of X-rays", J. Wiley & Son, N. Y., 1955 p. 116.

43. J. M. W. du Mond, Phys. Rev., 72, 83(1947).

44. V. Gerold, Acta Crystallogr., 10, 287 (1957).

45. S. Heine and J. Roppert, Acta Physica Austriaca, 15, 148 (1962).

46. S. Heine, Acta Physica Austriaca, 16, 144 (1963).

47. R. G. Stanton and W. D. Hoskins, "Numerical Analysis", in "Physical Chemistry", D. Henderson, Ed., Vol., XIA, Academic Press, N.Y., 1975.

48. A. C. R. Newbery, "Numerical Analysis", in "Handbook of Applied Mathematics", C. E. Pearson, Ed., Van Nostrand Reinhold, N.Y., 49. 1974.

49. L. E. Alexander, X-Ray Diffraction Methods in Polymer Science, Wiley Interscience, N. Y. (1969).

50. P. Debye, Am. Physik, 46, 809 (1915).

51. A. Guinier & G. Fournet, "Small Angle Scattering of X-Rays" (translated by C. B. Walker), J. Wiley & Sons, Inc., N.Y. (1955) p. 24.

52. Ibid, p. 127

53. Ibid, p. 149

54. Ibid, p. 70

55. O. Kratky and K. Schwarzkopf-Schier, Monatsch. Chem., 94, 714 (1963).

56. O. Kratky, I. Pilz and P. J. Schmitz, J. Colloid Interfoc. Sci., 21, 24 (1966).

57. G. Porod, Kolloid-Z., 124, 83 (1951).

58. P. Debye, H. R. Anderson, H. Brumberger, J. Appl. Phys., 28, 679 (1957).

59. V. Luzzati, J. Witz and A Nicolaieff, J. Mol. Biol., 3, 367 (1961).

60. W. Ruland, J. Appl. Cryst., 4, 70 (1971).

61. G. W. Brady, R. Salovey, J. Am. Chem. Soc., 86, 3499 (1964).

62. G. W. Brady, R. Salovey, J. M. Reddy, Biopol., 3, 573 (1965).

63. H. Li, B. Post, H. Morawetz, Makromol. Chem., 154, 89 (1972).

☆U.S.Government Printing Office: 1979 — 657-002/492